

Article

Phenomenology of the Composition of PM_{2.5} at an Urban Site in Northern France

Yamina Allouche, Marc Fadel , Amélie Ferté, Anthony Verdin, Frédéric Ledoux  and Dominique Courcot *

Unité de Chimie Environnementale et Interactions sur le Vivant (UCEIV) UR4492, Université du Littoral Côte d'Opale, F-59140 Dunkerque, France; yamina.allouche@univ-littoral.fr (Y.A.); marc.fadel@univ-littoral.fr (M.F.); amelie.ferte@univ-littoral.fr (A.F.); anthony.verdin@univ-littoral.fr (A.V.); frederic.ledoux@univ-littoral.fr (F.L.)

* Correspondence: dominique.courcot@univ-littoral.fr

Abstract: In this work, PM_{2.5} was sampled at Dunkerque, a medium-sized city located in northern France. The mean concentration of PM_{2.5} during the sampling period was $12.6 \pm 9.5 \mu\text{g}\cdot\text{m}^{-3}$. Samples were analyzed for elemental and organic carbon (EC/OC), water-soluble organic carbon (WSOC), humic-like substances (HULIS-C), water-soluble inorganic ions, and major and trace elements. The origin and the variations of species concentrations were examined using elemental enrichment factors, bivariate polar plot representations, and diagnostic concentration ratios. Secondary inorganic ions were the most abundant species (36% of PM_{2.5}), followed by OC (12.5% of PM_{2.5}). Secondary organic carbon (SOC) concentrations were estimated to account for 52% of OC. A good correlation between SOC and WSOC indicated that secondary formation processes significantly contribute to the WSOC concentrations. HULIS-C also represents almost 50% of WSOC. The determination of diagnostic ratios revealed the influence of anthropogenic emission sources such as integrated steelworks and fuel oil combustion. The clustering of 72 h air masses backward trajectories data evidenced that higher concentrations of PM_{2.5}, OC, and secondary inorganic aerosols were recorded when air masses came from north-eastern Europe and the French continental sector, showing the considerable impact of long-range transport on the air quality in northern France.

Keywords: PM_{2.5}; organic matter; humic-like substances; elements; tracers



Citation: Allouche, Y.; Fadel, M.; Ferté, A.; Verdin, A.; Ledoux, F.; Courcot, D. Phenomenology of the Composition of PM_{2.5} at an Urban Site in Northern France. *Atmosphere* **2024**, *15*, 603. <https://doi.org/10.3390/atmos15050603>

Academic Editors: Honglei Wang, Lijuan Shen and Xugeng Cheng

Received: 8 April 2024
Revised: 6 May 2024
Accepted: 8 May 2024
Published: 15 May 2024



Copyright: © 2024 by the authors. Licensee MDPI, Basel, Switzerland. This article is an open access article distributed under the terms and conditions of the Creative Commons Attribution (CC BY) license (<https://creativecommons.org/licenses/by/4.0/>).

1. Introduction

Fine particulate matter (PM_{2.5}) is drawing considerable attention from both the scientific community and public authorities due to its proven impacts on climate and human health. Indeed, several epidemiological studies have demonstrated the link between particulate air pollution and an increase in respiratory diseases, which can lead to premature death [1,2]. PM_{2.5} represents a complex mixture of carbonaceous species (organic matter (OM) containing water-soluble organic compounds, and elemental carbon (EC)), and inorganic substances such as water-soluble ions and major and trace elements. These species can be emitted by natural and/or anthropogenic sources. In urban areas, PM_{2.5} can be directly linked to both emissions by local sources and the contribution of long-range transport [3].

The Hauts-de-France region in France faces high PM concentrations due to various natural and anthropogenic sources, including domestic and industrial emissions [4]. The population in this region shows a respiratory disease and chronic obstructive pulmonary disease (COPD) related mortality rate up to 50% higher than the national average, according to the latest report from the Regional Health and Social Observatory [5]. Therefore, to take appropriate measures and limit exposure to PM, it is necessary to study their chemical composition and identify the sources that contribute to their concentration.

The chemical characterization of PM_{2.5} is highly variable and depends on several factors such as surrounding emission sources, meteorological conditions, and seasonal variations [6,7]. Studies in urban areas have revealed that water-soluble inorganic ions

are major components of fine particles and might generally contribute up to 50% [8]. Carbonaceous materials also contribute to a large fraction of $PM_{2.5}$ concentrations in the atmosphere [8–10]. Carbonaceous species are chemically divided into elemental carbon (EC) and organic carbon (OC). EC is mainly emitted by primary sources while OC appears both as primary organic carbon (POC) and secondary organic carbon (SOC). POC can be emitted from combustion processes, vehicular emissions, biomass burning, and cooking, as well as biogenic sources [11,12]. SOC can be formed either by the gas-to-particle oxidation of Volatile Organic Compounds (VOCs) or by oxidation reactions of organic matter in the particulate phase [13–18].

Organic matter contains a large number of water-soluble species with water-soluble organic carbon (WSOC) accounting for 30 to 70% of OC [19,20]. Among WSOC, water-soluble humic-like substances (HULIS) correspond to a group of organic compounds with characteristics similar to those of humic and fulvic acids [21]. They form a complex mixture of polycyclic structures containing hydroxyl, carboxyl, carbonyl, methoxy, and ester groups [22,23]. HULIS represent a significant fraction of organic aerosol. Indeed, the carbon content of HULIS (HULIS-C) accounts for 25 to 75% of WSOC [24,25]. Previous studies have identified that WSOC and HULIS-C result both from primary emissions such as biomass burning and atmospheric secondary reactions [22–24,26–28]. Kuang et al. [29] have also shown that secondary formation processes contribute to 69% of HULIS at an urban site in China. Moreover, WSOC can cause adverse health effects due to its ability to be absorbed into the lungs [30] and HULIS can be considered as a precursor of cloud droplets and can contribute to climate cooling [21]. Therefore, in-depth studies of the $PM_{2.5}$ carbonaceous fraction would be important because of the high impact on the atmospheric environment and human health. Furthermore, most of the studies dealing with air quality focus mainly on the inorganic and organic components of $PM_{2.5}$, omitting the water-soluble carbonaceous species, especially WSOC and HULIS-C. In western Europe, very few studies have focused on the carbonaceous fraction, including WSOC and HULIS-C [31–38]. In order to fill these gaps, this work has attempted to acquire a deeper knowledge of the chemical composition of $PM_{2.5}$, especially the carbonaceous fraction in a city influenced by local emissions (industries, road traffic, and domestic activities), located close to the North Sea, and impacted by emissions due to maritime traffic.

The main objective of this work was to study the chemical composition of $PM_{2.5}$, specifically the carbonaceous fraction with a focus on phenomena that could affect the composition of $PM_{2.5}$ in urban areas in northern France. Therefore, a sampling campaign was conducted in 2022 at Dunkerque. The collected samples were chemically analyzed to determine their composition in carbonaceous, ionic, and elemental fractions. The obtained data were analyzed using different tools in order to identify possible natural and anthropogenic sources that might contribute to $PM_{2.5}$ composition as well as to evaluate the impact of long-range transport during the sampling period. In this study, we report, for the first time for the Dunkerque site, results for the carbonaceous subfractions (OC and EC). Additionally, to the best of our knowledge, this study is the first to report results on the concentration levels of WSOC and HULIS-C in $PM_{2.5}$ in the northern France region as well as the identification of their possible emission sources. All of these results seek to deepen our understanding of PM sources in the region in order to support the development of effective emission reduction strategies.

2. Materials and Methods

2.1. Sampling Site Description

The sampling site was located in Dunkerque, a city in the north of France. Dunkerque is the fifth most populous city (193,000 inhabitants) in the Hauts-de-France region. The town is bordered by the North Sea and has the third-largest port in France, covering an area of over 70 km². The Dunkerque area is also under the influence of industrial emissions due to the presence of integrated steelworks (ISW), manganese alloys, and aluminum and aluminate production factories. Moreover, the southern part of the city is

connected to major highways (A25 and A16) with a high road traffic density (more than 30,000 vehicles/day, [39]). The sampling station was situated on the rooftop of the Lamar-tine University building (51°02′09″ N 2°22′51″ E) (Figure 1) in the city center of Dunkerque.

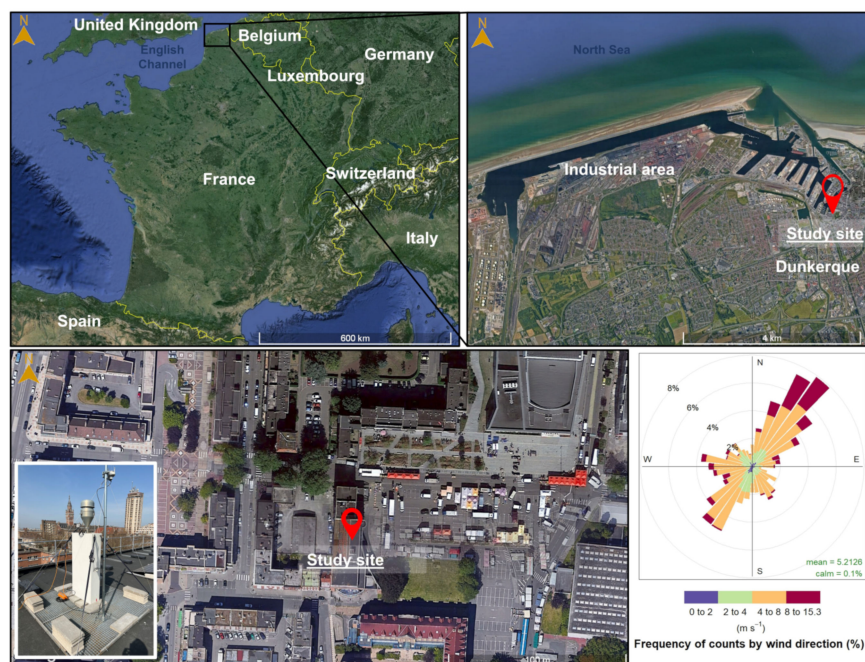


Figure 1. Location of the sampling site (modified from Google Earth) and wind rose representation for the sampling period (5 March to 8 July 2022).

2.2. Sampling Strategy

The sampling of PM_{2.5} was performed on a 24 h basis every day from 5 March to 8 July 2022. The samples were collected onto 150 mm pure quartz microfiber filters (PALL QAT-UP 2500) using a high-volume sampler DA80 (Digitel, Switzerland), operating at a flow rate of 30 m³·h⁻¹. The filters were pre-heated at 450 °C for 5 h to reduce organic impurities. Additionally, one field blank was gathered every fifteen days. A total of 120 PM_{2.5} samples and 8 field blanks were collected, wrapped in aluminum foil, and stored at −20 °C until chemical analysis. PM_{2.5} concentration data were obtained from the Atmo Hauts-de-France air quality monitoring network. Data from the Malo-les-Bains Atmo station, situated approximately 4 km from the sampling site, were used.

Meteorological data including temperature, pressure, hourly wind direction, and wind speed during the sampling period were obtained from the Infoclimat website, an open database for meteorological data in France “<http://infoclimat.com> (accessed on 8 January 2024)”. The sampling period was characterized by a mild and dry spring, followed by a sunny summer. The average temperatures during March, April, May, and June (rising from 14 °C to 22 °C) exceeded the normal monthly temperatures for the period 1991 to 2020 (8 °C to 16 °C, from March to June) “<http://infoclimat.com> (accessed on 8 January 2024)”. Moreover, there were several heatwaves in July. The wind rose presented in Figure 1 was drawn using the R software (R 4.2.3, Indianapolis, IN, USA) with the openair package by combining wind speeds and directions recorded every 30 min for all sampling days. Throughout the study period, winds predominately originated from the north-east sector, with the highest speeds being recorded in this direction (Figure 1). This observation reflects wind conditions typically encountered during the spring season. However, it contrasts with the annual wind patterns in the northern France region, which typically exhibit a predominance of south-west winds.

2.3. Analytical Procedures

PM_{2.5} samples as well as blank filters were analyzed for OC and EC, WSOC, HULIS-C, major and trace elements, and water-soluble ions. Analytical procedures are briefly described below. The concentrations of all identified species underwent correction by subtracting the mean value derived from the field blank filters.

2.3.1. OC and EC Analysis

OC and EC were measured on a 1.5 cm² punch of the quartz filter by a Sunset Laboratory OC/EC analyzer, which employed the thermal optical transmission method according to the EUSAAR-2 protocol [40].

2.3.2. Water-Soluble Ions, WSOC, and HULIS-C Analysis

A filter punch of 47 mm diameter for each sample was extracted three times with a few milliliters of ultrapure water by sonication for 30 min. Afterward, the leachates were gathered and filtered on nylon syringe filters (0.45 µm, Grosseron, Couëron, France) [41,42]. The extracts were then used to determine the concentrations of water-soluble HULIS-C, WSOC, and water-soluble ions.

The water-soluble HULIS-C fraction extraction is based on the solid phase extraction (SPE) method described by Lin et al. [23]. Briefly, the water extract was acidified with HCl to a pH of 2, then loaded on the SPE cartridge (Oasis HLB, 30 µm, 60 mg/cartridge, Waters, Milford, MA, USA). The cartridge was rinsed with 1 mL of ultrapure water, and the HULIS-C fraction was then eluted from the SPE cartridge with 2 mL of methanol. The eluate was evaporated to dryness under a gentle flow of nitrogen gas and re-dissolved in 10 mL of ultrapure water for analysis.

The WSOC and HULIS-C analysis was performed using a total organic carbon analyzer (TOC-V_{CSH}, Shimadzu, Kyoto, Japan). Samples were analyzed in triplicate and the concentrations were calculated as the average value of the three measurements. RSD values of less than 10% were obtained, indicating the repeatability of the analysis method. In order to assess the accuracy of the HULIS-C method, a standard reference material SRFA (Suwannee River Fulvic Acid) from the International Humic Substances Society (IHSS, Saint Paul, MN, USA) was used. A recovery rate of 93% was obtained, indicating the high efficiency of the extraction and the analysis method.

For the analysis of water-soluble ions, ion chromatography (DionexTM ICS-900, Thermo Scientific, Altrincham, Cheshire, UK) was used to quantify major anions (Cl⁻, SO₄²⁻, and NO₃⁻) and cations (Ca²⁺, Mg²⁺, K⁺, Na⁺, and NH₄⁺). The detection limits for ions varied between 0.17 and 0.78 ng·m⁻³. The ionic balance between total anions and total cations showed a linear correlation ($r^2 = 0.98$) with a slope close to 1, indicating the reliability of the analytical data.

2.3.3. Major and Trace Elements

Elemental analysis was performed using Inductively Coupled Plasma coupled with Atomic Emission Spectrometry (ICP–AES) and ICP coupled with Mass Spectrometry (ICP–MS). A detailed description of the procedure was reported in previous publications [41,42]. Briefly, for each sample, a 47 mm punch of the quartz filter was acid-digested with 5.5 mL of HNO₃/HF/HClO₄ (4/1/0.5; v/v/v) mixture in a PTFE flask at 120 °C overnight. Then, the acids were evaporated at 170 °C for 2 h to the last drop and ultrapure water was added to the residue. The obtained solution was diluted to 15 mL by adding ultrapure water, acidified to 2% by adding HNO₃, and then filtered on a cellulose acetate filter (0.45 µm, Grosseron, Couëron, France) before analysis. The ICP–AES, iCAP 6000 series, (Thermo Scientific, Altrincham, Cheshire, UK) was used to quantify Al, Ba, Ca, Fe, K, Mg, Na, P, S, Sr, and Zn while other trace elements (Ag, As, Cd, Cr, Cu, Mn, Ni, Pb, Rb, Sb, Sn, Ti, and V) were quantified using ICP–MS, (Agilent 7900, Santa Clara, CA, USA). Samples were analyzed in triplicate and the concentrations were calculated as the average value of the three measurements. RSD values of less than 10% were also obtained for these

analyses. The standard reference material NIST-SRM 1648a (urban particulate matter) from the National Institute of Standards and Technology (NIST, USA) was used to validate the analytical procedure. Recovery rates for the elemental quantification using ICP–AES and ICP–MS were within the acceptable range with values varying between 85% and 105% for all elements except for Cr (66%), Ni (110%), and Sb (115%). The detection limits varied between 0.003 and 1.63 ng·m^{−3} for ICP–AES and between 0.0002 and 0.04 ng·m^{−3} for ICP–MS.

2.4. Data Processing

The dataset used in this study corresponds to the concentrations of the different chemical species identified for the 120 samples. These include PM_{2.5}, OC, EC, WSOC, HULIS-C, inorganic ions (Cl[−], SO₄^{2−}, NO₃[−], Ca²⁺, Mg²⁺, K⁺, Na⁺, and NH₄⁺), and elements (Al, Ba, Ca, Fe, K, Mg, Na, P, S, Sr, Zn, Ag, As, Cd, Cr, Cu, Mn, Ni, Pb, Rb, Sb, Sn, Ti, and V).

2.4.1. Statistical Tests

In this study, the Shapiro–Wilk statistical test revealed that the concentration data of the different species did not comply with a normal distribution. Thus, the non-parametric Spearman correlation test was used in order to determine the correlation coefficient between different species. Two levels of significance were considered: $p < 0.01$ (99% confidence level) and $p < 0.001$ (99.9% confidence level).

2.4.2. Chemical Mass Closure

For the purpose of the chemical mass closure, PM_{2.5} was divided into different categories: sea-salt, crustal dust, secondary inorganic aerosols (SIA), organic matter (OM), elemental carbon (EC), and other elements that are not accounted for as minerals [43]. A detailed description of the calculation method is presented below.

The contribution of sea-salt was calculated by summing the six major ions [44]:

$$[\text{Sea-salt}] = ([\text{Na}^+] + [\text{ss-Cl}^-] + [\text{ss-Mg}^{2+}] + [\text{ss-K}^+] + [\text{ss-Ca}^{2+}] + [\text{ss-SO}_4^{2-}]) \quad (1)$$

with $[\text{ss-Cl}^-] = 1.79[\text{Na}^+]$; $[\text{ss-Mg}^{2+}] = 0.119[\text{Na}^+]$; $[\text{ss-K}^+] = 0.036[\text{Na}^+]$; $[\text{ss-Ca}^{2+}] = 0.038[\text{Na}^+]$; and $[\text{ss-SO}_4^{2-}] = 0.252[\text{Na}^+]$.

Ionic constituents such as Cl[−], Mg²⁺, K⁺, Ca²⁺, and SO₄^{2−} come from both marine and non-marine sources. Thus, it is necessary to discriminate sea-salt (ss) from non-sea-salt (nss) contributions. Assuming that all sodium ions are derived from marine origin, the sea-salt contribution can be determined on the basis of the composition of seawater.

The contribution of crustal dust was estimated by summing the concentrations of aluminum (Al), silicon (Si), non-sea-salt calcium (nss-Ca²⁺), iron (Fe), and titanium (Ti) [45]. Silicon was not measured in this study and its concentration was indirectly estimated from aluminum.

$$[\text{Crustal dust}] = 2.20[\text{Al}] + 2.49[\text{Si}] + 1.63[\text{nss-Ca}^{2+}] + 2.42[\text{Fe}] + 1.94[\text{Ti}] \quad (2)$$

with $[\text{Si}] = 3.92[\text{Al}]$ [46].

Secondary inorganic aerosols (SIA) correspond to the sum of NO₃[−], non-sea-salt SO₄^{2−} (nss-SO₄^{2−}), and NH₄⁺:

$$[\text{SIA}] = ([\text{NO}_3^-] + [\text{nss-SO}_4^{2-}] + [\text{NH}_4^+]) \quad (3)$$

with $[\text{nss-SO}_4^{2-}] = [\text{SO}_4^{2-}] - [\text{ss-SO}_4^{2-}]$.

To account for bound water, a hydration multiplication factor of 1.29 was applied to convert dry inorganic concentrations (sea-salt and SIA) into hydrated species [47,48].

Organic matter (OM) was calculated from organic carbon (OC), assuming a typical OM/OC ratio of 1.6 for urban areas [47,49,50].

The reconstructed PM_{2.5} mass corresponds to:

$$[\text{Reconstructed PM}_{2.5} \text{ mass}] = 1.29 \times [\text{sea-salt}] + 1.29 \times [\text{SIA}] + [\text{OM}] + [\text{EC}] + [\text{crustal dust}] + [\text{nss-Cl}^-] + [\text{nss-Mg}^{2+}] + [\text{nss-K}^+] + [\text{other elements}] \quad (4)$$

with [other elements] corresponding to the concentrations of all analyzed elements that were not taken into consideration in the previous equations.

2.4.3. Enrichment Factor for Major and Trace Elements

Enrichment factors (EFs) were determined in order to identify the relative contribution of crustal and anthropogenic sources to the levels of a specific element in PM_{2.5}. EFs were calculated using Ti as a reference element according to the following equation [51]:

$$\text{EF} = \frac{\left(\frac{C_x}{C_{\text{Ti}}}\right)_{\text{sample}}}{\left(\frac{C_x}{C_{\text{Ti}}}\right)_{\text{crustal}}} \quad (5)$$

where $\left(\frac{C_x}{C_{\text{Ti}}}\right)$ is the concentration ratio of the considered element (C_x) to Ti (C_{Ti}) in the PM_{2.5} samples divided by the same ratio for the upper continental crust as presented by Wedepohl [52]. An enrichment factor close to 1 suggested that the origin of the element is mainly crustal whereas a factor higher than 10 indicated that the element of interest originated from anthropogenic emission sources.

2.4.4. Estimation of Secondary Formation

The concentration of secondary organic carbon (SOC) was estimated using the EC tracer method as follows [53]:

$$\text{SOC} = \text{OC} - \left(\frac{\text{OC}}{\text{EC}}\right)_{\text{prim}} \times \text{EC} \quad (6)$$

where OC and EC are measured ambient concentrations and $\left(\frac{\text{OC}}{\text{EC}}\right)_{\text{prim}}$ represents a concentration ratio for primary combustion emission sources and was calculated as the 5th percentile of OC/EC data.

This same equation was used to estimate the concentrations of WSOC (WSOC_{sec}) [54] and HULIS-C_{sec} from secondary origins by replacing OC with WSOC and HULIS-C, respectively. To our knowledge, this is the first study that estimates the contribution of primary and secondary emissions to HULIS-C concentrations based on the EC tracer method.

2.4.5. Bivariate Polar Plots Representations

Bivariate polar plots were drawn using the open-source software R with the openair package [55]. These plots combine the concentration of PM_{2.5} components with the wind direction and wind speed. For each PM_{2.5} sample, concentration data obtained for the 24 h period were distributed amongst the 48 corresponding wind directions and speeds (one measurement every 30 min). Thus, the full dataset used to draw each polar plot counts 120 × 48 lines.

2.4.6. HYSPLIT Cluster Analysis

To study the long-range transport of PM_{2.5} and its components during the sampling period (5 March to 8 July 2022), 72 h air mass backward trajectories ending at the Dunkerque site were calculated every three hours by the Hybrid Single-Particle Lagrangian Integrated Trajectory model (HYSPLIT 5.3) [56]. Afterward, a cluster analysis using the same model was conducted by combining the 960 obtained trajectories into one single run.

3. Results and Discussions

3.1. Chemical Characterization of PM_{2.5} and Mass Reconstruction

3.1.1. PM_{2.5} Concentration and Composition

The average concentrations of PM_{2.5}, EC, OC, WSOC, water-soluble HULIS-C, water-soluble ions, and major and trace elements with an indication of their variability (standard deviations and minimum to maximum ranges) in the Dunkerque site during the sampling period are presented in Table 1.

Table 1. Concentrations of PM_{2.5} and its carbonaceous fraction, water-soluble ions, and major and trace elements during the sampling period ($n = 120$ samples; μ_A : arithmetic mean; μ_G : geometric mean; SD: standard deviation; Min: minimum value; and Max: maximum value). Values below detection limit were represented by “<D.L.”.

Species	μ_A	μ_G	Median	SD	Min	Max
PM _{2.5} ($\mu\text{g}\cdot\text{m}^{-3}$)	12.6	10.3	10.0	9.5	3.6	60.7
Carbonaceous fraction ($\mu\text{g}\cdot\text{m}^{-3}$)						
OC	1.6	1.3	1.4	1.2	0.1	9.4
WSOC	0.7	0.5	0.4	0.8	0.02	5.6
HULIS-C	0.4	0.1	0.2	0.5	<D.L.	3.1
EC	0.3	0.3	0.3	0.2	0.05	1.5
Water-soluble ions ($\mu\text{g}\cdot\text{m}^{-3}$)						
NO ₃ [−]	2.2	0.8	0.06	4.8	0.07	32.9
NH ₄ ⁺	1.1	0.7	0.6	1.7	0.06	11.7
SO ₄ ^{2−}	1.1	0.9	0.1	0.7	0.2	4.5
Ca ²⁺	0.2	0.04	0.08	0.2	<D.L.	1.3
Cl [−]	0.09	0.02	0.05	0.1	<D.L.	0.8
Na ⁺	0.06	0.03	0.04	0.05	<D.L.	0.3
K ⁺	0.04	0.01	0.02	0.08	<D.L.	0.6
Mg ²⁺	0.03	0.02	0.02	0.03	<D.L.	0.2
Major and trace elements ($\text{ng}\cdot\text{m}^{-3}$)						
Fe	114	56.9	59.0	135	<D.L.	653
Al	39.7	15.5	25.9	54.2	<D.L.	485
Zn	14.4	8.1	9.3	15.8	<D.L.	98.4
Mn	10.4	3.8	4.04	16.1	<D.L.	86.8
P	7.8	4.4	6.2	7.2	<D.L.	40.3
Pb	5.0	2.5	3.5	5.4	<D.L.	29.4
V	2.1	1.3	1.6	2.1	0.01	14.9
Ti	2.1	1.2	1.4	2.3	<D.L.	12.0
Ni	1.3	0.7	1.0	1.5	<D.L.	11.1
Cu	1.3	0.5	1.1	1.6	<D.L.	9.9
Ba	1.2	0.3	0.7	1.7	<D.L.	10.6
Sn	0.8	0.5	0.6	0.9	<D.L.	4.6
Sb	0.7	0.1	0.3	1.1	<D.L.	4.9
Cr	0.6	0.3	0.4	0.7	<D.L.	4.3
Rb	0.4	0.2	0.2	0.8	<D.L.	6.7
As	0.4	0.3	0.3	0.4	0.01	2.1
Sr	0.4	0.2	0.3	0.3	<D.L.	1.7
Nb	0.2	0.02	0.05	1.1	<D.L.	12.4
Tl	0.1	0.03	0.03	0.2	<D.L.	1.2
Cd	0.1	0.1	0.1	0.1	<D.L.	0.7
Co	0.1	0.04	0.05	0.06	<D.L.	0.3
Bi	0.08	0.05	0.1	0.08	<D.L.	0.6
Ce	0.08	0.05	0.1	0.07	<D.L.	0.4
La	0.05	0.03	0.05	0.05	<D.L.	0.2
Sc	0.04	0.02	0.01	0.06	<D.L.	0.4

The average concentration of PM_{2.5} measured by the Atmo Hauts-de-France air quality network during this period was $12.6 \pm 9.5 \mu\text{g}\cdot\text{m}^{-3}$, varying between 3.6 and $60.7 \mu\text{g}\cdot\text{m}^{-3}$. These values were therefore in line with the annual trend, where yearly average PM_{2.5} concentrations at the site ranged from 9 to $16 \mu\text{g}\cdot\text{m}^{-3}$, with an average value of $12 \mu\text{g}\cdot\text{m}^{-3}$ over the last ten years [57]. Moreover, the average PM_{2.5} concentration during the sampling period was lower than that obtained at the same site in 2010 ($33.2 \mu\text{g}\cdot\text{m}^{-3}$) and those reported (varying between 15 and $20 \mu\text{g}\cdot\text{m}^{-3}$) for other urban regions in Europe (France, Greece, and Italy) [44,58,59]. Furthermore, PM_{2.5} concentration was significantly lower than the values (varying between 70 and $100 \mu\text{g}\cdot\text{m}^{-3}$) recorded in Asian sites [60,61]. The differences in concentration levels might be mainly associated with higher population density, increased road traffic intensity, and industrial emissions.

In this study, the average PM_{2.5} concentration for the sampling period (four months) is lower than the annual limit value of $25 \mu\text{g}\cdot\text{m}^{-3}$ set by the European regulation (EU directive 2008/50/EC) [62]. However, the average PM_{2.5} concentration is two times higher than the World Health Organization (WHO) PM_{2.5} annual guideline value of $5 \mu\text{g}\cdot\text{m}^{-3}$ with 27% of sampling days recording concentrations exceeding the daily guideline value of $15 \mu\text{g}\cdot\text{m}^{-3}$ [63]. The highest concentrations of PM_{2.5} during the sampling period were recorded during pollution episodes, specifically during March (05/03, 21/03, 25/03, 26/03, and 29/03) where the concentrations ranged between 38.3 and $60.7 \mu\text{g}\cdot\text{m}^{-3}$.

The major constituents of PM_{2.5} were carbonaceous matter (OC and EC) as well as secondary inorganic ions (NH_4^+ , SO_4^{2-} , and NO_3^-), accounting together for 51% of the total PM_{2.5} mass (Table 1). Similar values to those obtained in Dunkerque have been reported for urban regions in Europe (varying between 44% and 52%) [44,58,64,65]. Furthermore, 25 major and trace elements were quantified in the PM_{2.5} samples with total concentrations ranging from 15 to $1033 \text{ng}\cdot\text{m}^{-3}$.

3.1.2. Carbonaceous Fraction of PM_{2.5}

The average concentrations of OC and EC at Dunkerque during the sampling period were $1.6 \pm 1.2 \mu\text{g}\cdot\text{m}^{-3}$ and $0.3 \pm 0.2 \mu\text{g}\cdot\text{m}^{-3}$, respectively (Table 1). Within the organic fraction, the mean concentration of WSOC was $0.7 \pm 0.8 \mu\text{g}\cdot\text{m}^{-3}$, and the average concentration of HULIS-C was $0.4 \pm 0.5 \mu\text{g}\cdot\text{m}^{-3}$. The (min to max) ranges of concentrations of these carbonaceous subfractions also exhibited large variability: 0.1– $9.4 \mu\text{g}\cdot\text{m}^{-3}$ for OC, 0.05– $1.5 \mu\text{g}\cdot\text{m}^{-3}$ for EC, 0.02– $5.6 \mu\text{g}\cdot\text{m}^{-3}$ for WSOC, and <D.L.– $3.1 \mu\text{g}\cdot\text{m}^{-3}$ for HULIS-C. The average concentrations for both OC and EC were in the lower range of values (0.5 – $4.5 \mu\text{g}\cdot\text{m}^{-3}$ for OC and 0.04 – $1.5 \mu\text{g}\cdot\text{m}^{-3}$ for EC) reported for different sites in Europe (France, Italy, Greece, Finland, Netherlands, Belgium, and Czech Republic) [47,65–68]. The higher OC and EC values obtained at some sites could be explained by the seasonal variations as well as the typology of the sites. Several studies have shown that higher concentrations of OC and EC were observed in winter compared to summer [68–71]. This could be explained by PM emissions from combustion processes for domestic heating in winter but also by adverse meteorological conditions leading to poorer dispersion of pollutants in the atmosphere [68].

The mean concentrations of WSOC and HULIS-C were also lower than those obtained in urban and suburban environments in Europe (0.5 to $1.8 \mu\text{g}\cdot\text{m}^{-3}$ for WSOC and 0.5 to 1.4 for HULIS-C) [31,32,36,38,50,72–74]. Higher concentrations of WSOC and HULIS-C were measured in urban sites particularly affected by biomass burning [31,75]. Moreover, WSOC and HULIS-C concentrations also vary depending on the seasons, with a higher influence of residential heating in winter and secondary formation processes enhanced by high temperatures in summer [31,32,76]. Thus, several papers have highlighted that the lowest WSOC and HULIS-C concentrations have been reported in spring [8,77].

3.1.3. Concentrations of Inorganic Ions

The total concentration of inorganic ions was $4.9 \mu\text{g}\cdot\text{m}^{-3}$, contributing to 38.8% of the PM_{2.5} mass (Table 1). Secondary inorganic ions (NO_3^- , NH_4^+ , and SO_4^{2-}) were

the dominant components of PM_{2.5}, accounting for 17.9%, 9.1%, and 8.9%, respectively, followed by Ca²⁺ (1.2%), Cl⁻ (0.7%), Na⁺ (0.5%), K⁺ (0.3%), and Mg²⁺ (0.3%).

Secondary inorganic ions are formed by the gas-particle conversion processes of their corresponding precursors (NO_x, SO₂, and NH₃) in the atmosphere [78]. The neutralization ratio between NH₄⁺ and the sum of NO₃⁻ and SO₄²⁻ was close to 1, suggesting that ammonium is predominately found in the atmosphere as ammonium nitrate and ammonium sulfate. The evaluation of the concentration ratios between SO₄²⁻ and NH₄⁺ on one hand and SO₄²⁻ + NO₃⁻ and NH₄⁺ on the other hand indicates that ammonium nitrate (66%) is approximately twice as abundant as ammonium sulfate (34%). This trend has already been observed at Cap Gris-Nez, a site in the north of France [79].

Na⁺ is used as a reference to determine sea-salt components in aerosol particles and to assess the enrichment of some ions in the marine environment. In general, the Cl⁻/Na⁺ ratio value in fresh marine aerosols is 1.79 [80,81]. In our study, the average Cl⁻/Na⁺ ratio was equal to 0.98, which is indicative of chloride depletion and aged sea-salt [81,82]. However, some of the samples exhibited a Cl⁻/Na⁺ ratio value higher than 1.8, leading to the assumption that Cl⁻ is not completely of marine origins and might be also emitted from anthropogenic sources such as biomass burning and industrial emissions [83]. According to the location of the study site, biomass burning could be suggested as a potential source to explain the non-marine origins of Cl⁻, as well as the emissions from the ISW located close to the sampling site [84].

Furthermore, the assessment of the concentration ratios involving Mg²⁺ (Mg²⁺/Na⁺ = 0.42), K⁺ (K⁺/Na⁺ = 1.05), and Ca²⁺ (Ca²⁺/Na⁺ = 3.8) in comparison with Na⁺ showed values higher than the ones encountered in fresh sea-salt (Mg²⁺/Na⁺ = 0.12, K⁺/Na⁺ = 0.04, and Ca²⁺/Na⁺ = 0.04). These findings also highlighted the significant contribution of non-marine origins for these ions which could be related to dust sources including both natural crustal origins and industrial ones [85]. A study conducted by Hleis et al. [84] investigated the chemical profiles of dust emissions from the integrated iron and steel plant in Dunkerque. They found high levels of calcium in the sintering area, primarily in the form of CaCO₃, while emissions from the sintering stack were dominated by KCl content.

3.1.4. Concentrations of Major and Trace Elements

The average concentrations of the 25 analyzed elements in PM_{2.5} in the Dunkerque site during the sampling period are summarized in Table 1. The sum of the studied elements was 0.2 µg·m⁻³, corresponding approximately to 1.6% of the PM_{2.5} mass. The substantial standard deviation of observed values suggested significant variability in concentrations, which might be due to meteorological conditions. The highest concentrations were attributed to Fe, Al, and Zn, accounting for 84% of elemental concentration. Moreover, other elements, such as Mn, P, and Pb, contributed significantly to elemental concentrations. Atmospheric concentrations of the remaining trace elements were below 5 ng·m⁻³. The average concentrations of V and Ni were lower than the values (1.7 to 5.7 ng·m⁻³) usually observed in the region [41,79,86]. The results were comparable to the findings reported in the literature for other European cities [87] but lower than the values found in east-Mediterranean sites (total elemental concentration higher than 2.6 µg·m⁻³) [49,88]. This is mainly due to the fact that the east-Mediterranean sites were highly affected by road traffic emissions as well as dust storm episodes from the Saharan and the Arabian deserts, leading to higher concentrations in crustal elements.

3.1.5. Chemical Mass Closure of PM_{2.5}

Chemical mass closure of PM_{2.5} was performed using the approach described in Section 2.4.2 in order to estimate the contribution of the different components to the total PM_{2.5} concentrations. The measured and reconstructed PM_{2.5} concentrations were strongly correlated (r² = 0.96) with a slope of 0.8 (Figure S1), indicating that the method used was able to accurately reconstruct the PM_{2.5} concentrations based on its chemical characteristics. However, during pollution episodes (5 March and 25 March), an overestimation of reconstructed

PM_{2.5} was observed, which can be explained by higher NO₃⁻ concentrations during these days (28.5 and 32.9 μg·m⁻³, respectively).

The distribution of the concentrations of various PM_{2.5} chemical components during each month of the sampling period is shown in Figure 2. During the total period, the reconstructed PM_{2.5} mass included 46% of SIA, 20.3% of OM, 8% of crustal dust, 2.4% of EC, 1.4% of sea-salts, and 0.8% of nss-ions (nss-K⁺, nss-Cl⁻, and nss-Mg²⁺). During the sampling period, PM_{2.5} in Dunkerque was mainly composed of SIA and OM. This observation was consistent with results obtained in the region and more generally in western Europe [74,89].

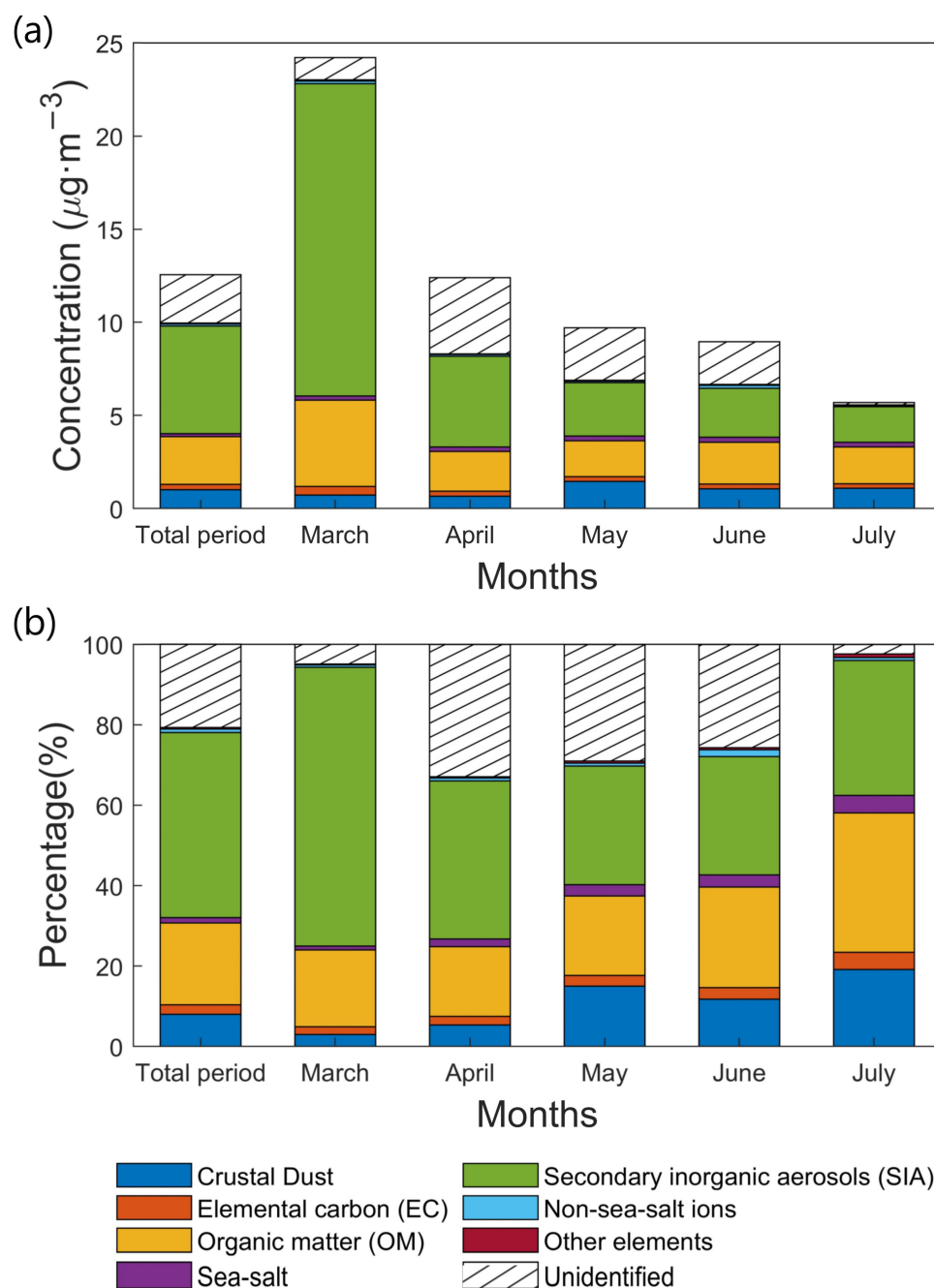


Figure 2. The reconstructed chemical composition of PM_{2.5} (expressed (a) in μg·m⁻³ and (b) in % of PM_{2.5} concentration) during every sampling month (from March to June (full month) and July (8 days)) and the total sampling period in Dunkerque.

When evaluating the monthly evolution of these components, SIA was the largest contributor to PM_{2.5} during the spring months with a share of 69.3%, 39.3%, and 29.5% during

March, April, and May, respectively. Nitrate displays the highest concentrations in spring, especially in March, a period usually associated with PM pollution episodes in western Europe and dominated by secondary inorganic aerosols [90]. According to Petit et al. [90], atmospheric circulation favoring dry conditions during spring might enhance the risk of pollution events. During pollution episodes in this month (March), the contribution of nitrate to PM_{2.5} concentrations was high and varied between 35 and 60%.

OM was the second important contributor to PM_{2.5}. However, large variations in OM monthly average concentrations occurred between March (4.6 $\mu\text{g}\cdot\text{m}^{-3}$) and the other months (about 2.0 $\mu\text{g}\cdot\text{m}^{-3}$). High OM concentrations in March are usually attributed to enhanced emissions from the combustion process for domestic heating [46,69].

The mean crustal dust concentrations were higher during May (1.4 $\mu\text{g}\cdot\text{m}^{-3}$), June (1.1 $\mu\text{g}\cdot\text{m}^{-3}$), and July (1.1 $\mu\text{g}\cdot\text{m}^{-3}$) than in March (0.7 $\mu\text{g}\cdot\text{m}^{-3}$) and April (0.7 $\mu\text{g}\cdot\text{m}^{-3}$). These higher concentrations during these months could be associated with dust resuspension [91]. However, we cannot exclude the industrial influence since some elements (Al and Fe) used in the calculations of crustal dust could also be linked to anthropogenic sources [41,84].

Sea-salt, EC, and nss-ions represented a minor fraction of the total PM_{2.5}. About 80% of the PM_{2.5} mass was identified (Figure 2), which is in line with the literature (50 to 80%) [92–94]. The unresolved mass could be explained by moisture content, non-analyzed compounds, as well as the uncertainty resulting from approximate conversion factor calculations [89].

3.2. Identifying Sources of Emissions

3.2.1. Diagnostic Ratios of Elements and Enrichment Factors

In order to identify possible anthropogenic emission sources of elements in PM_{2.5}, enrichment factors (EFs) were calculated using Ti as reference element (Figure 3). The EFs obtained for Ce, Sr, Nb, Ba, La, K, and Mg were below 10, suggesting a predominance of crustal origins (Figure 3).

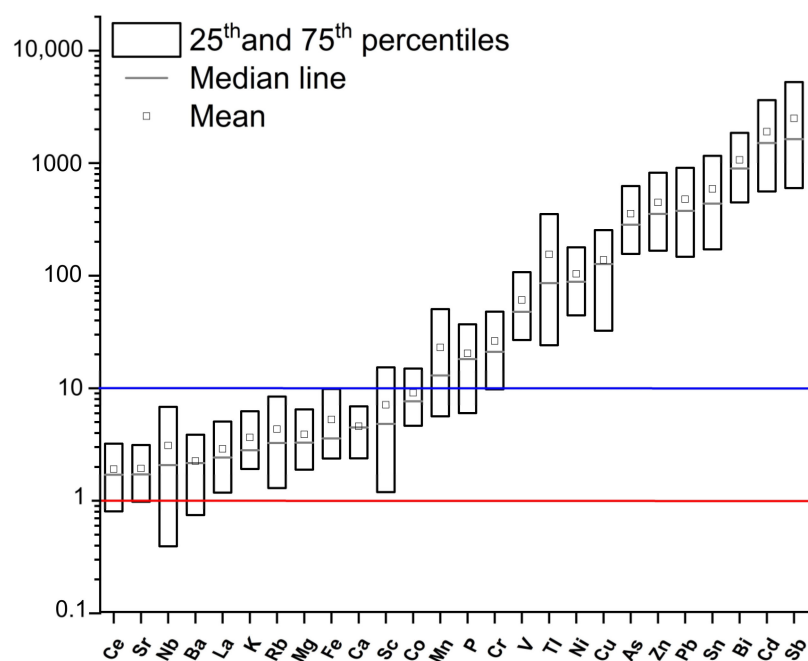


Figure 3. Elemental enrichment factors represented as boxplots (median value, 25th and 75th percentiles, and mean value (as a square)) in PM_{2.5} collected in Dunkerque using Ti as a reference element. Elements with EF values close to 1 (red line) were mainly attributed to crustal origins while those with an EF higher than 10 (blue line) have significant proportions coming from anthropogenic emission sources.

Moderate EFs ($10 \leq EF \leq 100$) were recorded for Fe, Sc, Co, Mn, P, Cr, V, Ti, and Ni. V and Ni were commonly linked to heavy fuel oil combustion (HFO) either from industrial or shipping activities [79,95]. The latter source can be identified by a concentration ratio of V/Ni ranging from 2.3 to 4.5 as well as a V/EC ratio of less than 2 [96,97]. In this study, the average V/Ni and V/EC concentration ratios were 2.3 and 0.1, respectively, consistent with HFO combustion from shipping activities in Sulphur Emission Control Areas (SECA). Moreover, the bivariate polar plots of these elements (Figure S2) were similar with the highest concentrations recorded when the wind blew from the west-northwest and north-northeast sectors. These results were consistent with the literature data and the position of the study area near the North Sea, suggesting that these elements were associated with HFO combustion from shipping activities in the region.

EFs between 100 and 1000 were observed for Cu, As, Zn, Pb, Sn, and Bi. As, Pb, and Zn have previously been identified as emitted from the steel production activity in the Dunkerque area [86]. On the other hand, Zn, Pb, Cu, and Sn could be associated with non-exhaust road traffic emissions and more precisely from wear of vehicle tires and brakes [98–100]. According to Alves et al. [98], As and Cu could also be emitted from metallurgical industries. Bi is mainly associated with fossil fuel combustion, ferromanganese alloys, and aluminum production [101,102].

The highest EFs (>1000) were found for Cd and Sb. Antimony is used in the manufacture of brake linings (Sb_2S_3) to reduce vibration and improve friction stability, so it is commonly used as a brake wear tracer [103,104]. Generally, the Cu/Sb ratio (ranging from 1.13 to 8.33) was used as a chemical tracer for brake wear-related emissions [105–107]. In this study, a Cu/Sb ratio of 2.3 was obtained, indicating that brake wear most likely is a source of these elements. Cd, in addition to other elements such as Fe, Al, Zn, Mn, Pb, and Rb, is mainly linked to emissions from ISW [86]. Based on the bivariate polar plots of different elements presented in Figure S2, the highest concentrations of these elements were observed when the wind blew from the west-northwest sector. This sector likely represents the industrial influence, suggesting that emissions from industrial activities contribute significantly to the levels of these elements in the atmosphere. Similar observations were also made in previous studies in Dunkerque where these elements were mainly emitted from iron and steelwork facilities [41,84]. In order to further highlight the influence of the integrated steelworks, a selection of samples collected under winds blowing from the ISW direction was obtained (samples collected under the $250\text{--}320^\circ$ wind sector) (Figure S3). The elemental ratios calculated for these samples ($Zn/Fe = 0.1$, $Zn/Mn = 1.2$, $Rb/Cr = 1.2$, and $Pb/Cr = 12.4$) were consistent with the ratios obtained in a previous study conducted in Dunkerque for samples collected downwind of the industrial area ($Zn/Fe = 0.1$, $Zn/Mn = 1.7$, $Rb/Cr = 0.9$, and $Pb/Cr = 12$) [41].

3.2.2. Diagnostic Ratios and Correlations between Carbonaceous Species

The correlation between carbonaceous species was studied and the scatter plots are presented in Figure S4. Concerning the correlation between OC and EC, two extreme correlation trends with slopes of 2.9 and 7.8 can be distinguished alongside the average trend with a slope of 5.5 (Figure S4a). This suggests that OC and EC may originate from multiple sources. According to the literature, ratio values within the range of 0.3 and 1 have been attributed to light- and heavy-duty vehicles running on diesel, values between 1.4 and 5 have been ascribed to gasoline catalyst light-duty vehicles, while ratios between 1.1 and 14.5 to biomass burning sources, and between 33 and 82 to cooking emissions [108–110]. In this study, the range of the OC/EC concentration ratios found implied that traffic exhaust emissions might not be the dominant emission source of carbonaceous matter at Dunkerque during the sampling period.

The average OC/EC concentration ratio of 5.5 suggests the presence of biomass burning sources in the study area, contributing to the $PM_{2.5}$ concentrations. This hypothesis is supported by the enrichment of K^+ , recognized as an inorganic tracer of biomass burning. Moreover, the assessment of the $nss\text{-}K^+/EC$ ratio in this study (0.2) falls within the range

identified in the literature for biomass burning (0.2–1.1) [111]. Furthermore, the polar plot representation of K^+ shows that higher concentrations were observed in the south-eastern (SE) sector with low wind speed (Figure S5). This is in line with the representation of the OC/EC ratio, where values between 5 and 6 were recorded in the SE sector (Figure 4). Biomass burning sources related to the use of wood combustion for domestic heating is an important contributor to PM during the cold season at urban sites in France [112,113]. Previous studies in Europe have observed a large contribution of wood burning such as 20% of the total $PM_{2.5}$ in Paris (France) [114], up to 80% in Oslo (Norway) [115], 47% of all Danish $PM_{2.5}$ emissions [116], and 24% in Helsinki (Finland) [117].

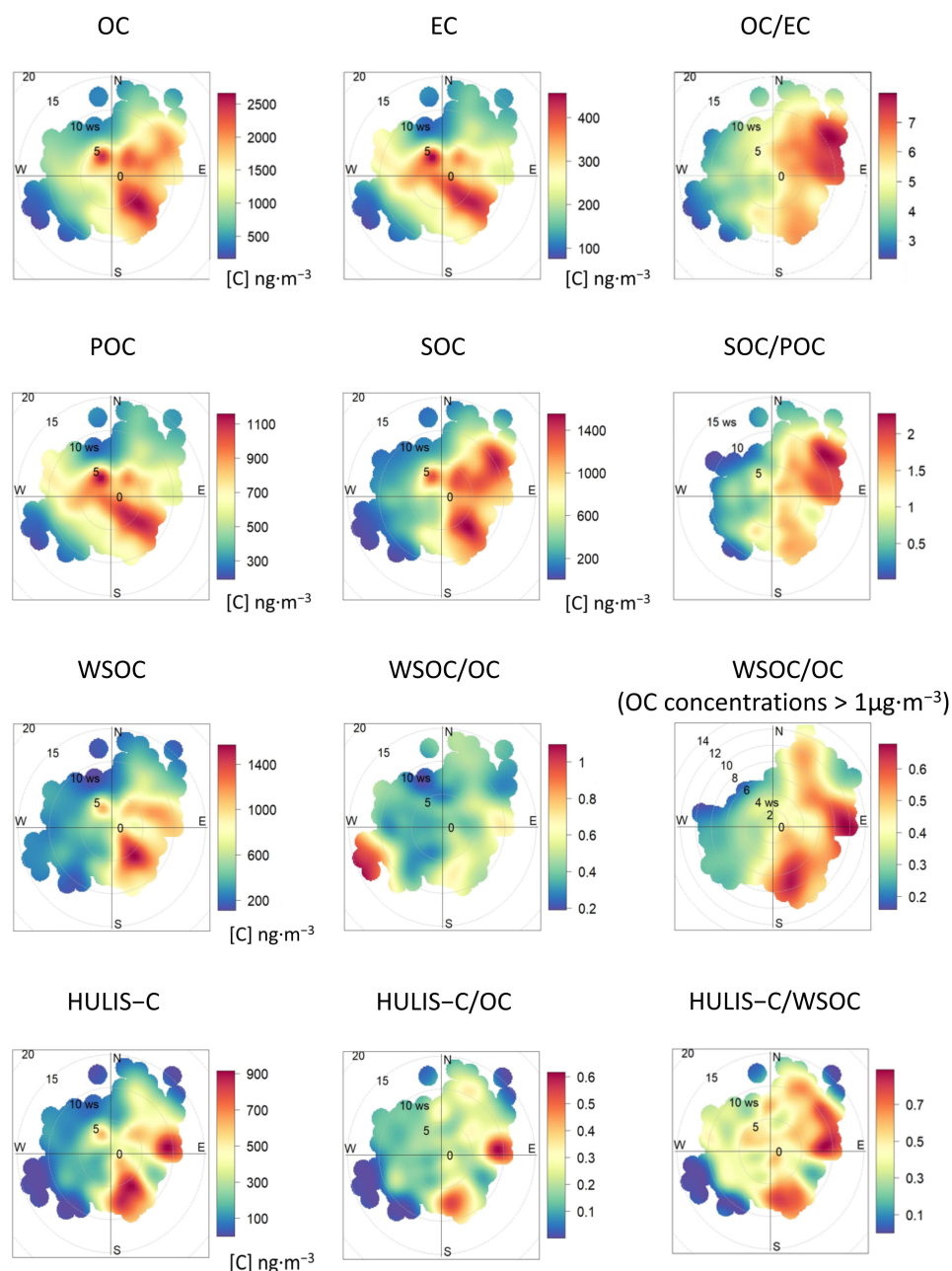


Figure 4. Bivariate polar plots of the carbonaceous species concentrations (expressed in $ng \cdot m^{-3}$) as well as concentration ratios in $PM_{2.5}$ collected at Dunkerque during the sampling period (5 March to 8 July 2022).

High concentrations of OC and EC were observed under south-easterly (SE) winds and also under north-easterly (NE) winds for OC, consisting mainly of continental air masses.

The OC/EC polar plot (Figure 4) shows that maximum values (higher than 7) were observed in the north-east (NE) sector when wind speeds were higher than $10 \text{ m}\cdot\text{s}^{-1}$. The elevated ratios observed in the NE sector were mainly due to the low EC concentrations in this wind direction. Furthermore, the high OC/EC ratios under NE sector might be either due to the accumulation of pollutants on the trajectory of the air mass under anticyclonic conditions or the potential impact of the long-range transport of organic aerosols [66,118,119]. Conversely, the polar plot representation of OC/EC indicated that the lowest OC/EC ratios were recorded for winds originating from the south-western (SW) sector, with speeds exceeding $10 \text{ m}\cdot\text{s}^{-1}$. These winds consist mainly of marine winds passing over the Atlantic Ocean and the English Channel (Figure 4).

A strong positive correlation between WSOC and OC ($r^2 = 0.88$) may indicate that WSOC and OC have a similar source (Figure S4b) [8,120]. The average value of the WSOC/OC ratio (0.42) was consistent with other studies conducted in urban areas (WSOC/OC ratio value varying between 0.2 and 0.5) and indicated the influence of biomass burning [8,36,121]. In addition, the WSOC/OC ratio could also be used as an indicator of the formation of secondary organic aerosols (SOA) [8,26]. The increase in this ratio value could be due to the photochemical transformation of primary organic aerosols (POA) to WSOC and/or the formation of water-soluble secondary organic aerosols via gas-to-particle conversion. In our case, the WSOC/OC ratio value decreased from 0.6 to 0.2 from March to July, which means that WSOC was mainly of secondary origins during winter and early spring [122]. The WSOC/OC polar plot presented in Figure 4 revealed that the highest values of the ratio (between 0.8 and 0.95) were observed for winds originating from the SW sector with high wind speeds (higher than $10 \text{ m}\cdot\text{s}^{-1}$). Upon closer examination of the $\text{PM}_{2.5}$ samples collected under these specific conditions (three samples), it was noted that they exhibited the lowest concentrations of OC, which could explain the high value of the ratio. On the other hand, and in the same wind sector and for wind speeds lower than $10 \text{ m}\cdot\text{s}^{-1}$, moderate (0.5–0.6) to low (0.2–0.3) WSOC/OC concentration ratios were recorded. When considering samples with OC concentrations higher than $1 \mu\text{g}\cdot\text{m}^{-3}$, the WSOC/OC representation showed that the highest ratios were observed in the NE and SE wind directions.

The strong correlation between OC and HULIS-C ($r^2 = 0.76$) (Figure S4c), as well as WSOC and HULIS-C ($r^2 = 0.83$) (Figure S4d), suggested that these species share common sources such as biomass burning and secondary formation to the carbonaceous species in $\text{PM}_{2.5}$ [30]. The fraction of HULIS-C in WSOC was 48.2%. This result is in agreement with other studies worldwide showing that HULIS-C accounted for about half of WSOC in urban areas [24,29,31,35,37,123]. The HULIS-C/ $\text{PM}_{2.5}$ (2.9%) and HULIS-C/OC ratio (22.2%) values were slightly lower than those obtained in some previous studies in urban sites [24,27]. It is interesting to note that the HULIS-C/OC polar plot (Figure 4) showed two spots under northeasterly and southeasterly sectors (such as the HULIS-C polar plot), corresponding to a ratio value of 0.6 approximately. This latter value is consistent with the ratio observed in biomass burning-influenced ambient aerosol samples (close to 0.6), which is higher than the one observed for fresh biomass burning emissions (0.34 ± 0.05) [124].

To determine the influence of secondary formation, the concentrations of secondary organic carbon (SOC) were calculated based on Equation (6). Figure 5 shows the concentrations of SOC and POC (Figure 5a) and their contributions to the concentration of OC (Figure 5b). The mean concentration of SOC was $0.8 \mu\text{g}\cdot\text{m}^{-3}$, varying between 0.01 and $5.7 \mu\text{g}\cdot\text{m}^{-3}$ (Figure 5a). Therefore, SOC accounted on average for 52% of OC and 7% of $\text{PM}_{2.5}$. The temporal variation showed that the highest proportion of SOC to OC was observed in early June (Figure 5b). Our results were quite similar with other findings, showing that SOC accounted for approximately 56% of OC and 10% of $\text{PM}_{2.5}$ in the urban atmosphere [120,125]. Additionally, the average SOC/POC concentration ratio value during the study period was 1.2 and varied between 0.1 and 4.7. For the whole period, the partitioning of POC and SOC varied without following any particular seasonal trend. However, the upward trend in average temperatures between March and July (14 to $22 \text{ }^\circ\text{C}$) would suggest an increase in the SOC/POC ratio during the transition from

late winter (early March) to early summer (July), as observed in other studies [120,126,127]. Indeed, this is explained by the effect of the increase in temperature and intensity of solar radiation, which favors the formation of SOC [20,120]. Furthermore, it is interesting to note an increase in the SOC/POC concentration ratio value for winds coming from the north-east sector (Figure 4). The rise in OC content was also observed under northeasterly winds which corresponds to anticyclonic conditions in the region. This scenario appears to correspond to meteorological conditions suitable for favoring the conversion of primary organic compounds into secondary ones.

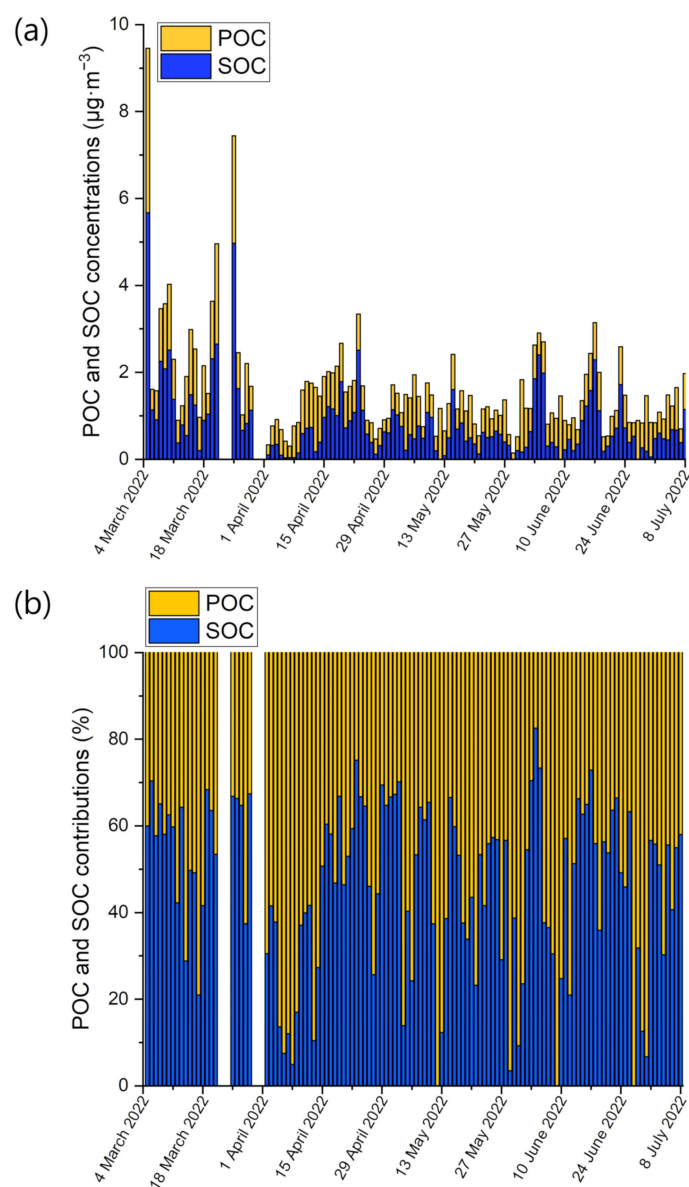


Figure 5. Temporal variations of (a) the concentrations of SOC and POC (expressed in $\text{ng}\cdot\text{m}^{-3}$) and (b) their relative contribution to OC concentrations during the sampling period in Dunkerque.

WSOC and HULIS-C constituted an important part of secondary organic carbon (SOC). The correlations between SOC and WSOC ($r^2 = 0.86$), as well as SOC and HULIS-C ($r^2 = 0.71$) concentrations (Figure S6), indicated that the formation of SOA was a major factor determining the WSOC and HULIS-C concentrations in the study area. Thus, the proportion of secondary WSOC_{sec} and HULIS-C_{sec} as well as primary WSOC_{pri} and HULIS-C_{pri} has been determined (Section 2.4.4). WSOC_{sec} and HULIS_{sec} represent 89% and 93% of WSOC and HULIS-C, respectively. The highest concentration of WSOC_{sec} ($3.9 \mu\text{g}\cdot\text{m}^{-3}$) and HULIS_{sec}

($0.7 \mu\text{g}\cdot\text{m}^{-3}$) was observed in March. The bivariate polar plot of SOC (Figure 4) shows that high levels of secondary compounds were observed mainly for NE and SE winds.

3.3. Back Trajectories Analysis

72 h backward trajectories of air masses ending at the Dunkerque site every three hours were established using the HYSPLIT model [56] and subsequently clustered (eight back trajectories per sampling date). The air mass back trajectories observed during the sampling period can be decomposed into five clusters (Figure 6): 28% of back trajectories originated from north-eastern Europe (cluster 1), 18% from the French continental sector (cluster 2), 19% from the Atlantic Ocean and English Channel (cluster 3), 18% from the Atlantic Ocean and crossing the United Kingdom (cluster 4), and 16% from the North Sea (Cluster 5). In order to associate $\text{PM}_{2.5}$ concentrations and their constituents to the different clusters, the choice was made to only consider $\text{PM}_{2.5}$ samples having eight back trajectories, covering the 24 h sampling time, associated with the same cluster. A total of 65 $\text{PM}_{2.5}$ samples among the 120 ones collected met the criteria and were distributed into the five different clusters. The average concentrations of $\text{PM}_{2.5}$, its main components (sea-salt, crustal dust, SIA, EC, OM, WSOC, and HULIS-C), as well as different concentration ratios (OC/EC, WSOC/OC, and SOC/POC) were calculated for each cluster and are presented in Table 2 in order to evaluate their long-range origins. The highest concentration levels of $\text{PM}_{2.5}$ and SIA ($22.2 \mu\text{g}\cdot\text{m}^{-3}$ and $10.3 \mu\text{g}\cdot\text{m}^{-3}$ respectively) were attributed to cluster 1 and mainly associated with continental air masses that come from north-eastern Europe. Additionally, the highest $\text{PM}_{2.5}$ concentrations, associated with pollution episodes, were also found in this cluster.

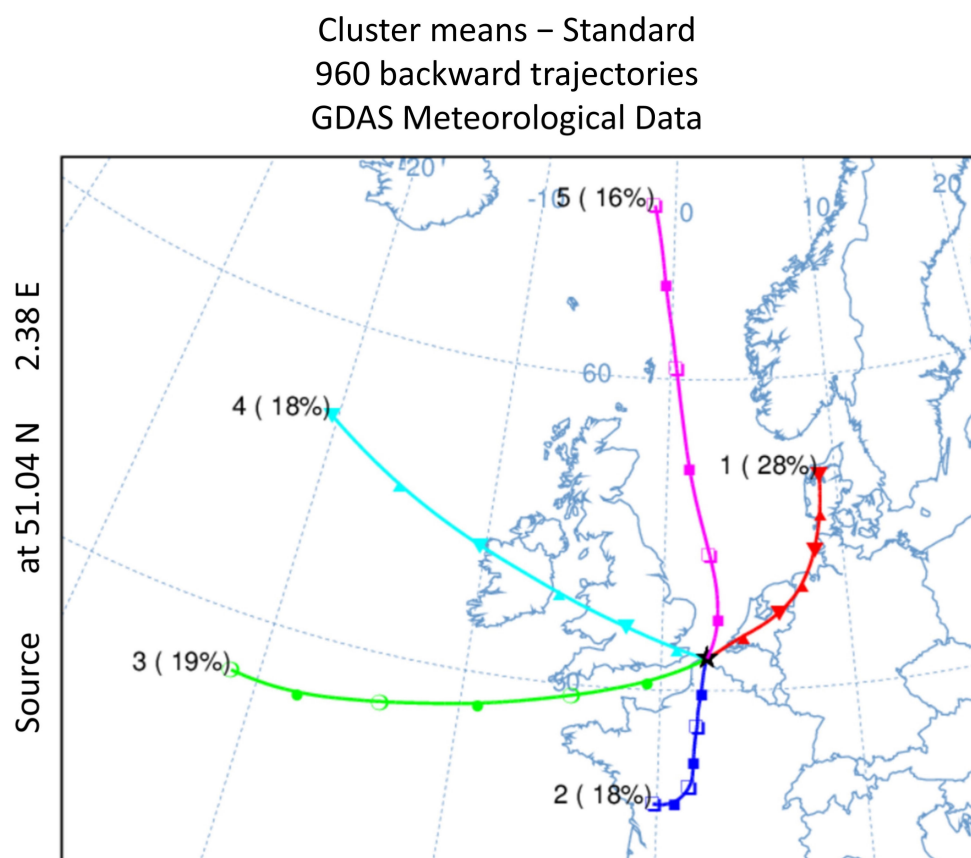


Figure 6. HYSPLIT cluster analysis for the sampling days from March to July 2022.

The large contribution of SIA in cluster 1 as well as cluster 2 indicated either their regional origins or that of their gas precursors. They were associated with long-range and continental transport of anthropogenic sources [79,90]. These findings align with the works

of Potier et al. [128], in which receptor-based models and chemistry transport modeling highlighted the important and recurrent impact of the “Near-East” regions (including Belgium, Netherlands, and Germany, etc.) on PM concentrations in the north of France. For the carbonaceous matter, important concentrations of EC and OC (including SOC, WSOC, and HULIS-C) were recorded for PM_{2.5} associated with cluster 1 mass trajectories and also cluster 2 (French continental sector). In western Europe, it has been estimated that about 70% of OC concentrations originate from long-range transport [129]. Moreover, the high OC/EC concentration ratio value as well as the SOC/POC ratio and the WSOC/OC ratio found for PM_{2.5} samples associated with clusters 1 and 2 highlighted once again the impact of biomass combustion in south-western France and north-eastern Europe [116] as well as the influence of secondary formation processes on the carbonaceous fraction. These findings were also underscored in the polar plot representations of the concentration ratios of OC/EC and WSOC/OC, indicating a clear prevailing direction in the NE and SE sectors, respectively, with high winds (Figure 4). According to Waked et al. [113], higher OC/EC concentration ratios were found during exceedance days, which could be partly related to secondary formation. These photochemical processes are enhanced by high-pressure systems, which in western Europe correspond to air masses originating from the continental sector.

Table 2. Average concentrations in $\mu\text{g}\cdot\text{m}^{-3}$ of PM_{2.5}, OM, WSOC, HULIS-C, SOC, EC, SIA, sea-salt, and crustal dust as well as the concentration ratios of OC/EC, WSOC/OC, and SOC/POC for PM_{2.5} samples according to their origin defined by the cluster number (values in bold might be indicative of long-range transport).

Clusters	1	2	3	4	5
PM _{2.5}	22.2	13.0	6.9	8.3	12.0
OM	4.4	3.0	1.5	2.1	1.8
WSOC	1.6	0.9	0.2	0.5	0.5
HULIS-C	0.8	0.5	0.1	0.4	0.3
SOC	1.8	0.9	0.3	0.6	0.6
EC	0.4	0.4	0.3	0.3	0.2
SIA	10.3	4.2	1.5	2.0	3.8
Sea-salt	0.1	0.1	0.5	0.2	0.2
Crustal dust	0.9	0.7	1.5	1.3	0.7
OC/EC	7.1	5.2	3.3	4.8	5.2
WSOC/OC	0.6	0.5	0.2	0.4	0.5
SOC/POC	1.8	1.0	0.6	0.9	0.7

Meanwhile, clusters 3, 4, and 5, characterized by a strong marine influence, correspond to the lowest PM_{2.5} concentrations (C3: 6.9 $\mu\text{g}\cdot\text{m}^{-3}$, C4: 8.3 $\mu\text{g}\cdot\text{m}^{-3}$, C5: 12 $\mu\text{g}\cdot\text{m}^{-3}$). In addition to that, the lowest SOC/POC ratios were observed for clusters 3 and 5 and might be attributed to the contribution of shipping activities over the English Channel and the North Sea.

4. Conclusions

The main objective of this work was to identify phenomena that can affect the composition of PM_{2.5} in an urban site, located in northern France. In order to achieve that, PM_{2.5} was sampled at Dunkerque, from March to July 2022. The chemical composition of PM_{2.5} was determined, focusing mainly on carbonaceous, elemental, and ionic fractions. Throughout the sampling period, the site was affected by several pollution episodes characterized by elevated concentrations of PM_{2.5} as well as secondary inorganic aerosols. These episodes, predominantly observed in March, were attributed to the long-range transport of pollutants originating from north-eastern European countries as well as from the French continental sector. The influence of industrial activities on PM_{2.5} concentration has also been revealed. Indeed, the highest concentration levels of Fe, Zn, Mn, Cd, and Rb were recorded downwind of the emissions from a local integrated steelworks and manganese

alloys plant. The elemental ratios calculated ($Zn/Fe = 0.1$, $Zn/Mn = 1.2$, $Rb/Cr = 1.2$, and $Pb/Cr = 12.4$) also confirmed the impact of the integrated steelworks emissions. On the other hand, the diagnostic concentration ratios of OC/EC (5.5) and $WSOC/OC$ (0.4), as well as K^+/EC (0.2), revealed the influence of biomass burning on $PM_{2.5}$ concentrations. Secondary organic carbon accounted for 52% of OC and 7% of $PM_{2.5}$. Additionally, 89% of WSOC and 93% of HULIS-C were of secondary origins. These results revealed also that the secondary formation processes were significant contributors to $PM_{2.5}$ and its major components such as OC, WSOC, and HULIS-C. Finally, back trajectories analysis showed that the north-eastern Europe (28%) and the French continental (18%) sectors were important hotspots for $PM_{2.5}$ concentrations, especially for SIA, EC, and OC (including SOC, WSOC, and HULIS-C), showing the potential influence of long-range transport on the air quality in Dunkerque. Overall, this study highlighted the main sources of $PM_{2.5}$ in Dunkerque, showing the complexity between local and regional influences. Future studies should focus on a longer sampling campaign in order to further exploit the seasonal effect, in addition to quantifying the contribution of these sources to ambient $PM_{2.5}$ concentrations in order to develop effective mitigation policies.

Supplementary Materials: The following Supporting Information can be downloaded at: <https://www.mdpi.com/article/10.3390/atmos15050603/s1>. Figure S1: Correlations between $PM_{2.5}$ reconstructed by mass closure and $PM_{2.5}$ measured (expressed in $ng \cdot m^{-3}$); Figure S2: Bivariate polar plots of elemental concentration at Dunkerque during sampling period; Figure S3: Windrose representation for the selection of sampling days that were influenced by industrial emissions (samples collected under the $250\text{--}320^\circ$ wind sector); Figure S4: Correlations between the concentrations of (a) OC and EC, (b) WSOC and OC, (c) OC and HULIS-C and (d) WSOC and HULIS-C; Figure S5: Bivariate polar plots of K^+ concentration at Dunkerque during sampling period; Figure S6: Correlations between the concentrations of (a) SOC and WSOC, and (b) SOC and HULIS-C.

Author Contributions: Conceptualization, Y.A., M.F., A.V., F.L. and D.C.; methodology, Y.A., M.F., F.L. and D.C.; software, Y.A., M.F. and F.L.; validation, Y.A., M.F., F.L. and D.C.; formal analysis, Y.A. and M.F.; investigation, Y.A. and A.F.; writing—original draft preparation, Y.A.; writing—review and editing, M.F., A.V., F.L. and D.C.; supervision, M.F., F.L. and D.C.; project administration, D.C.; funding acquisition, D.C. All authors have read and agreed to the published version of the manuscript.

Funding: This work has been produced within the French Program “Territoires d’Innovations: Dunkerque, l’Energie Créative” framework, which has received funding from the “Grand Plan d’Investissement”. The work also involves the Health Services “Espace Santé du Littoral” and “Observatoire Local de Santé”.

Institutional Review Board Statement: Not applicable.

Informed Consent Statement: Not applicable.

Data Availability Statement: The data presented in this study are available on request from the corresponding author. The data are not publicly available as it is a part of a thesis study of a student.

Acknowledgments: The authors thank the Institut Chevreul (Université de Lille) for the analysis of metals by ICP–MS, Dorothée Dewaele (Centre Commun de Mesures, ULCO) for her help in the ICP–AES analysis, and also Amaury Kasproviak (ULCO) for his help in the ionic chromatography analysis.

Conflicts of Interest: The authors declare no conflicts of interest.

References

1. Apte, J.S.; Marshall, J.D.; Cohen, A.J.; Brauer, M. Addressing Global Mortality from Ambient $PM_{2.5}$. *Environ. Sci. Technol.* **2015**, *49*, 8057–8066. [[CrossRef](#)]
2. Burnett, R.; Chen, H.; Szyszkowicz, M.; Fann, N.; Hubbell, B.; Pope, C.A.; Apte, J.S.; Brauer, M.; Cohen, A.; Weichenthal, S.; et al. Global Estimates of Mortality Associated with Long-Term Exposure to Outdoor Fine Particulate Matter. *Proc. Natl. Acad. Sci. USA* **2018**, *115*, 9592–9597. [[CrossRef](#)] [[PubMed](#)]
3. Pandolfi, M.; Mooibroek, D.; Hopke, P.; van Pinxteren, D.; Querol, X.; Herrmann, H.; Alastuey, A.; Favez, O.; Hüglin, C.; Perdrix, E.; et al. Long-Range and Local Air Pollution: What Can We Learn from Chemical Speciation of Particulate Matter at Paired Sites? *Atmos. Chem. Phys.* **2020**, *20*, 409–429. [[CrossRef](#)]

4. Europe's Air Quality Status 2022—European Environment Agency. Available online: <https://www.eea.europa.eu/publications/status-of-air-quality-in-Europe-2022/europes-air-quality-status-2022> (accessed on 12 September 2022).
5. OR2S Diagnostic Territorialisé Des Hauts-de-France—Territoires de Proximité. Available online: http://or2s.fr/images/PRS/2017_DiagnosticTerritorialiséDesHautsDeFrance_PRS2_HautsDeFrance.pdf (accessed on 5 March 2024).
6. Juda-Rezler, K.; Reizer, M.; Maciejewska, K.; Błaszczak, B.; Klejnowski, K. Characterization of Atmospheric PM_{2.5} Sources at a Central European Urban Background Site. *Sci. Total Environ.* **2020**, *713*, 136729. [[CrossRef](#)] [[PubMed](#)]
7. Błaszczak, B.; Juda-Rezler, K.; Rogula-Kozłowska, W.; Reizer, M.; Mathews, B.; Maciejewska, K.; Klejnowski, K. Ionic Composition of Fine Particulate Matter from Urban and Regional Background Sites in Poland. *Environ. Eng. Sci.* **2017**, *34*, 236–250. [[CrossRef](#)]
8. Xiang, P.; Zhou, X.; Duan, J.; Tan, J.; He, K.; Yuan, C.; Ma, Y.; Zhang, Y. Chemical Characteristics of Water-Soluble Organic Compounds (WSOC) in PM_{2.5} in Beijing, China: 2011–2012. *Atmos. Res.* **2017**, *183*, 104–112. [[CrossRef](#)]
9. Correa-Ochoa, M.A.; Bedoya, R.; Gómez, L.M.; Aguiar, D.; Palacio-Tobón, C.A.; Colorado, H.A. A Review on the Characterization and Measurement of the Carbonaceous Fraction of Particulate Matter. *Sustainability* **2023**, *15*, 8717. [[CrossRef](#)]
10. Massabò, D.; Prati, P. An Overview of Optical and Thermal Methods for the Characterization of Carbonaceous Aerosol. *Riv. Nuovo Cimento* **2021**, *44*, 145–192. [[CrossRef](#)]
11. Abbas, I.; Badran, G.; Verdin, A.; Ledoux, F.; Roumié, M.; Courcot, D.; Garçon, G. Polycyclic Aromatic Hydrocarbon Derivatives in Airborne Particulate Matter: Sources, Analysis and Toxicity. *Environ. Chem. Lett.* **2018**, *16*, 439–475. [[CrossRef](#)]
12. Samaké, A.; Jaffrezo, J.-L.; Favez, O.; Weber, S.; Jacob, V.; Canete, T.; Albinet, A.; Charron, A.; Riffault, V.; Perdrix, E.; et al. Arabitol, Mannitol, and Glucose as Tracers of Primary Biogenic Organic Aerosol: The Influence of Environmental Factors on Ambient Air Concentrations and Spatial Distribution over France. *Atmos. Chem. Phys.* **2019**, *19*, 11013–11030. [[CrossRef](#)]
13. Shrivastava, M.; Cappa, C.D.; Fan, J.; Goldstein, A.H.; Guenther, A.B.; Jimenez, J.L.; Kuang, C.; Laskin, A.; Martin, S.T.; Ng, N.L.; et al. Recent Advances in Understanding Secondary Organic Aerosol: Implications for Global Climate Forcing. *Rev. Geophys.* **2017**, *55*, 509–559. [[CrossRef](#)]
14. Kroll, J.H.; Seinfeld, J.H. Chemistry of Secondary Organic Aerosol: Formation and Evolution of Low-Volatility Organics in the Atmosphere. *Atmos. Environ.* **2008**, *42*, 3593–3624. [[CrossRef](#)]
15. Fadel, M.; Ledoux, F.; Farhat, M.; Kfoury, A.; Courcot, D.; Afif, C. PM_{2.5} Characterization of Primary and Secondary Organic Aerosols in Two Urban-Industrial Areas in the East Mediterranean. *J. Environ. Sci.* **2021**, *101*, 98–116. [[CrossRef](#)] [[PubMed](#)]
16. Mahilang, M.; Deb, M.K.; Pervez, S. Biogenic Secondary Organic Aerosols: A Review on Formation Mechanism, Analytical Challenges and Environmental Impacts. *Chemosphere* **2021**, *262*, 127771. [[CrossRef](#)] [[PubMed](#)]
17. Hallquist, M.; Wenger, J.C.; Baltensperger, U.; Rudich, Y.; Simpson, D.; Claeys, M.; Dommen, J.; Donahue, N.M.; George, C.; Goldstein, A.H.; et al. The Formation, Properties and Impact of Secondary Organic Aerosol: Current and Emerging Issues. *Atmos. Chem. Phys.* **2009**, *9*, 5155–5236. [[CrossRef](#)]
18. Dai, H.; Huang, G.; Zeng, H. Multi-Objective Optimal Dispatch Strategy for Power Systems with Spatio-Temporal Distribution of Air Pollutants. *Sustain. Cities Soc.* **2023**, *98*, 104801. [[CrossRef](#)]
19. Chen, P.; Kang, S.; Tripathee, L.; Ram, K.; Rupakheti, M.; Panday, A.; Zhang, Q.; Guo, J.; Wang, X.; Pu, T.; et al. Light Absorption Properties of Elemental Carbon (EC) and Water-Soluble Brown Carbon (WS-BrC) in the Kathmandu Valley, Nepal: A 5-Year Study. *Environ. Pollut.* **2020**, *261*, 114239. [[CrossRef](#)] [[PubMed](#)]
20. Zhang, Y.-L.; El-Haddad, I.; Huang, R.-J.; Ho, K.-F.; Cao, J.-J.; Han, Y.; Zotter, P.; Bozzetti, C.; Daellenbach, K.R.; Slowik, J.G.; et al. Large Contribution of Fossil Fuel Derived Secondary Organic Carbon to Water Soluble Organic Aerosols in Winter Haze in China. *Atmos. Chem. Phys.* **2018**, *18*, 4005–4017. [[CrossRef](#)]
21. Graber, E.R.; Rudich, Y. Atmospheric HULIS: How Humic-like Are They? A Comprehensive and Critical Review. *Atmos. Chem. Phys.* **2006**, *6*, 729–753. [[CrossRef](#)]
22. Fan, X.; Song, J.; Peng, P. Comparison of Isolation and Quantification Methods to Measure Humic-like Substances (HULIS) in Atmospheric Particles—ScienceDirect. *Atmos. Environ.* **2012**, *60*, 366–374. [[CrossRef](#)]
23. Lin, P.; Huang, X.; He, L.; Yu, J. Abundance and Size Distribution of HULIS in Ambient Aerosols at a Rural Site in South China. *J. Aerosol Sci.* **2010**, *41*, 74–87. [[CrossRef](#)]
24. Tao, Y.; Sun, N.; Li, X.; Zhao, Z.; Ma, S.; Huang, H.; Ye, Z.; Ge, X. Chemical and Optical Characteristics and Sources of PM_{2.5} Humic-Like Substances at Industrial and Suburban Sites in Changzhou, China. *Atmosphere* **2021**, *12*, 276. [[CrossRef](#)]
25. Ye, Z.; Li, Q.; Ma, S.; Zhou, Q.; Gu, Y.; Su, Y.; Chen, Y.; Chen, H.; Wang, J.; Ge, X. Summertime Day-Night Differences of PM_{2.5} Components (Inorganic Ions, OC, EC, WSOC, WSON, HULIS, and PAHs) in Changzhou, China. *Atmosphere* **2017**, *8*, 189. [[CrossRef](#)]
26. Sun, T.; Li, R.; Meng, Y.; Han, Y.; Cheng, H.; Fu, H. Size-Segregated Atmospheric Humic-Like Substances (HULIS) in Shanghai: Abundance, Seasonal Variation, and Source Identification. *Atmosphere* **2021**, *12*, 526. [[CrossRef](#)]
27. Li, X.; Han, J.; Hopke, P.K.; Hu, J.; Shu, Q.; Chang, Q.; Ying, Q. Quantifying Primary and Secondary Humic-like Substances in Urban Aerosol Based on Emission Source Characterization and a Source-Oriented Air Quality Model. *Atmos. Chem. Phys.* **2019**, *19*, 2327–2341. [[CrossRef](#)]
28. Mayol-Bracero, O.; Guyon, P.; Graham, B.; Roberts, G.; Andreae, M.; Decesari, S.; Facchini, M.; Sandro, F.; Artaxo, P. Water-Soluble Organic Compounds in Biomass Burning Aerosols over Amazonia: 2. Apportionment of the Chemical Composition and Importance of the Polyacidic Fraction. *J. Geophys. Res.* **2002**, *107*, LBA-14. [[CrossRef](#)]

29. Kuang, B.Y.; Lin, P.; Huang, X.H.H.; Yu, J.Z. Sources of Humic-like Substances in the Pearl River Delta, China: Positive Matrix Factorization Analysis of PM_{2.5} Major Components and Source Markers. *Atmos. Chem. Phys.* **2015**, *15*, 1995–2008. [CrossRef]
30. Lee, J.S.; Kim, E.S.; Kim, K.-A.; Yu, J.Z.; Kim, Y.P.; Jung, C.H.; Lee, J.Y. Temporal Variations and Characteristics of the Carbonaceous Species in PM_{2.5} Measured at Anmyeon Island, a Background Site in Korea. *Asian J. Atmos. Environ.* **2020**, *14*, 35–46. [CrossRef]
31. Baduel, C.; Voisin, D.; Jaffrezo, J.-L. Seasonal Variations of Concentrations and Optical Properties of Water Soluble HULIS Collected in Urban Environments. *Atmos. Chem. Phys.* **2010**, *10*, 4085–4095. [CrossRef]
32. Frka, S.; Grgić, I.; Turšič, J.; Gini, M.I.; Eleftheriadis, K. Seasonal Variability of Carbon in Humic-like Matter of Ambient Size-Segregated Water Soluble Organic Aerosols from Urban Background Environment. *Atmos. Environ.* **2018**, *173*, 239–247. [CrossRef]
33. Guilhermet, J.; Preunkert, S.; Voisin, D.; Baduel, C.; Legrand, M. Major 20th Century Changes of Water-Soluble Humic-like Substances (HULISWS) Aerosol over Europe Inferred from Alpine Ice Cores. *J. Geophys. Res. Atmos.* **2013**, *118*, 3869–3878. [CrossRef]
34. Kristensen, T.; Du, L.; Nguyen, Q.; Nøjgaard, J.; Bender Koch, C.; Nielsen, O.; Hallar, A.; Lowenthal, D.; Nekat, B.; Pinxteren, D.; et al. Chemical Properties of HULIS from Three Different Environments. *J. Atmos. Chem.* **2015**, *72*, 65–80. [CrossRef]
35. Krivácsy, Z.; Kiss, G.; Ceburnis, D.; Jennings, G.; Maenhaut, W.; Salma, I.; Shooter, D. Study of Water-Soluble Atmospheric Humic Matter in Urban and Marine Environments. *Atmos. Res.* **2008**, *87*, 1–12. [CrossRef]
36. López-Caravaca, A.; Crespo, J.; Galindo, N.; Yubero, E.; Juárez, N.; Nicolás, J.F. Sources of Water-Soluble Organic Carbon in Fine Particles at a Southern European Urban Background Site. *Atmos. Environ.* **2023**, *306*, 119844. [CrossRef]
37. Voliotis, A.; Prokeš, R.; Lammel, G.; Samara, C. New Insights on Humic-like Substances Associated with Wintertime Urban Aerosols from Central and Southern Europe: Size-Resolved Chemical Characterization and Optical Properties. *Atmos. Environ.* **2017**, *166*, 286–299. [CrossRef]
38. Witkowska, A.; Lewandowska, A.U. Water Soluble Organic Carbon in Aerosols (PM₁, PM_{2.5}, PM₁₀) and Various Precipitation Forms (Rain, Snow, Mixed) over the Southern Baltic Sea Station. *Sci. Total Environ.* **2016**, *573*, 337–346. [CrossRef] [PubMed]
39. Hauts-de-France, Cartes de Trafics Annuels. Available online: <https://www.hauts-de-france.developpement-durable.gouv.fr/?Cartes-de-trafics-annuels> (accessed on 28 March 2024).
40. Cavalli, F.; Viana, M.; Yttri, K.E.; Genberg, J.; Putaud, J.-P. Toward a Standardised Thermal-Optical Protocol for Measuring Atmospheric Organic and Elemental Carbon: The EUSAAR Protocol. *Atmos. Meas. Tech.* **2010**, *3*, 79–89. [CrossRef]
41. Kfoury, A.; Ledoux, F.; Roche, C.; Delmaire, G.; Roussel, G.; Courcot, D. PM_{2.5} Source Apportionment in a French Urban Coastal Site under Steelworks Emission Influences Using Constrained Non-Negative Matrix Factorization Receptor Model. *J. Environ. Sci.* **2016**, *40*, 114–128. [CrossRef] [PubMed]
42. Ledoux, F.; Courcot, L.; Courcot, D.; Aboukaïs, A.; Puskaric, E. A Summer and Winter Apportionment of Particulate Matter at Urban and Rural Areas in Northern France. *Atmos. Res.* **2006**, *82*, 633–642. [CrossRef]
43. Chow, J.C.; Lowenthal, D.H.; Chen, L.-W.A.; Wang, X.; Watson, J.G. Mass Reconstruction Methods for PM_{2.5}: A Review. *Air Qual. Atmos. Health* **2015**, *8*, 243–263. [CrossRef]
44. Bressi, M.; Sciare, J.; Ghersi, V.; Bonnaire, N.; Nicolas, J.B.; Petit, J.-E.; Moukhtar, S.; Rosso, A.; Mihalopoulos, N.; Féron, A. A One-Year Comprehensive Chemical Characterisation of Fine Aerosol (PM_{2.5}) at Urban, Suburban and Rural Background Sites in the Region of Paris (France). *Atmos. Chem. Phys.* **2013**, *13*, 7825–7844. [CrossRef]
45. Huang, X.H.H.; Bian, Q.; Ng, W.M.; Louie, P.K.K.; Yu, J.Z. Characterization of PM_{2.5} Major Components and Source Investigation in Suburban Hong Kong: A One Year Monitoring Study. *Aerosol Air Qual. Res.* **2014**, *14*, 237–250. [CrossRef]
46. Esmaeilirad, S.; Lai, A.; Abbaszade, G.; Schnelle-Kreis, J.; Zimmermann, R.; Uzu, G.; Daellenbach, K.; Canonaco, F.; Hassankhany, H.; Arhami, M.; et al. Source Apportionment of Fine Particulate Matter in a Middle Eastern Metropolis, Tehran-Iran, Using PMF with Organic and Inorganic Markers. *Sci. Total Environ.* **2020**, *705*, 135330. [CrossRef] [PubMed]
47. Genga, A.; Ielpo, P.; Siciliano, T.; Siciliano, M. Carbonaceous Particles and Aerosol Mass Closure in PM_{2.5} Collected in a Port City. *Atmos. Res.* **2017**, *183*, 245–254. [CrossRef]
48. Sciare, J.; Oikonomou, K.; Cachier, H.; Mihalopoulos, N.; Andreae, M.O.; Maenhaut, W.; Sarda-Estève, R. Aerosol Mass Closure and Reconstruction of the Light Scattering Coefficient over the Eastern Mediterranean Sea during the MINOS Campaign. *Atmos. Chem. Phys.* **2005**, *5*, 2253–2265. [CrossRef]
49. Fakhri, N.; Fadel, M.; Öztürk, F.; Keleş, M.; Iakovides, M.; Pikridas, M.; Abdallah, C.; Karam, C.; Sciare, J.; Hayes, P.L.; et al. Comprehensive Chemical Characterization of PM_{2.5} in the Large East Mediterranean-Middle East City of Beirut, Lebanon. *J. Environ. Sci.* **2023**, *133*, 118–137. [CrossRef] [PubMed]
50. Galindo, N.; Yubero, E.; Clemente, A.; Nicolás, J.F.; Navarro-Selma, B.; Crespo, J. Insights into the Origin and Evolution of Carbonaceous Aerosols in a Mediterranean Urban Environment. *Chemosphere* **2019**, *235*, 636–642. [CrossRef] [PubMed]
51. Chester, R.; Murphy, K.J.T.; Lin, F.J.; Berry, A.S.; Bradshaw, G.A.; Corcoran, P.A. Factors Controlling the Solubilities of Trace Metals from Non-Remote Aerosols Deposited to the Sea Surface by the ‘Dry’ Deposition Mode. *Mar. Chem.* **1993**, *42*, 107–126. [CrossRef]
52. Hans Wedepohl, K. The Composition of the Continental Crust. *Geochim. Cosmochim. Acta* **1995**, *59*, 1217–1232. [CrossRef]
53. Lim, H.-J.; Turpin, B.J.; Edgerton, E.; Hering, S.V.; Allen, G.; Maring, H.; Solomon, P. Semicontinuous Aerosol Carbon Measurements: Comparison of Atlanta Supersite Measurements. *J. Geophys. Res. Atmos.* **2003**, *108*, 8419. [CrossRef]
54. Zhang, X.; Zhang, X.; Talifu, D.; Ding, X.; Wang, X.; Abulizi, A.; Zhao, Q.; Liu, B. Secondary Formation and Influencing Factors of WSOC in PM_{2.5} over Urumqi, NW China. *Atmos. Environ.* **2023**, *293*, 119450. [CrossRef]

55. Carslaw, D. OpenAir Manual | PDF | R (Programming Language) | Data Analysis. Available online: <https://www.scribd.com/document/366730673/OpenAir-Manual> (accessed on 3 April 2024).
56. Draxler, R.; Stunder, B.; Rolph, G.; Stein, A.; Taylor, A.; Zinn, S.; Loughner, C.; Crawford, A. HYSPLIT User's Guide. 2023. Available online: https://www.arl.noaa.gov/documents/reports/hysplit_user_guide.pdf (accessed on 12 February 2024).
57. Atmo Hauts-de-France Mesures Des Stations | Atmo Hauts-de-France. Available online: <https://www.atmo-hdf.fr/accéder-aux-données/mesures-des-stations> (accessed on 28 March 2024).
58. Cesari, D.; Donato, A.; Conte, M.; Merico, E.; Giangreco, A.; Giangreco, F.; Contini, D. An Inter-Comparison of PM_{2.5} at Urban and Urban Background Sites: Chemical Characterization and Source Apportionment. *Atmos. Res.* **2016**, *174–175*, 106–119. [CrossRef]
59. Kassomenos, P.A.; Vardoulakis, S.; Chaloulakou, A.; Paschalidou, A.K.; Grivas, G.; Borge, R.; Lumbrellas, J. Study of PM₁₀ and PM_{2.5} Levels in Three European Cities: Analysis of Intra and Inter Urban Variations. *Atmos. Environ.* **2014**, *87*, 153–163. [CrossRef]
60. Shikha; Rajouriya, K.; Pipal, A.S.; Taneja, A. Chemical Characterization and Health Risk Assessment of Particulate Matter Near National Highway at Urban and Semi-Urban Locations of Northern India. *Aerosol Sci. Eng.* **2023**, *7*, 517–533. [CrossRef]
61. Liu, Z.; Gao, W.; Yu, Y.; Hu, B.; Xin, J.; Sun, Y.; Wang, L.; Wang, G.; Bi, X.; Zhang, G.; et al. Characteristics of PM_{2.5} Mass Concentrations and Chemical Species in Urban and Background Areas of China: Emerging Results from the CARE-China Network. *Atmos. Chem. Phys.* **2018**, *18*, 8849–8871. [CrossRef]
62. European Council. On Ambient Air Quality and Cleaner Air for Europe 2008/50/EC. *Off. J. Eur. Union* **2008**, *1*, 1–44.
63. World Health Organization. *WHO Global Air Quality Guidelines: Particulate Matter (PM_{2.5} and PM₁₀), Ozone, Nitrogen Dioxide, Sulfur Dioxide and Carbon Monoxide*; World Health Organization: Geneva, Switzerland, 2021; ISBN 978-92-4-003422-8.
64. Blaszcak, B.; Rogula-Kozłowska, W.; Mathews, B.; Juda-Rezler, K.; Klejnowski, K.; Rogula-Kopiec, P. Chemical Compositions of PM_{2.5} at Two Non-Urban Sites from the Polluted Region in Europe. *Aerosol Air Qual. Res.* **2016**, *16*, 2333–2348. [CrossRef]
65. Remoundaki, E.; Kassomenos, P.; Mantas, E.; Mihalopoulos, N.; Tsezos, M. Composition and Mass Closure of PM_{2.5} in Urban Environment (Athens, Greece). *Aerosol Air Qual. Res.* **2013**, *13*, 72–82. [CrossRef]
66. Friman, M.; Aurela, M.; Saarnio, K.; Teinilä, K.; Kesti, J.; Harni, S.D.; Saarikoski, S.; Hyvärinen, A.; Timonen, H. Long-Term Characterization of Organic and Elemental Carbon at Three Different Background Areas in Northern Europe. *Atmos. Environ.* **2023**, *310*, 119953. [CrossRef]
67. Hama, S.; Ouchen, I.; Wyche, K.P.; Cordell, R.L.; Monks, P.S. Carbonaceous Aerosols in Five European Cities: Insights into Primary Emissions and Secondary Particle Formation. *Atmos. Res.* **2022**, *274*, 106180. [CrossRef]
68. Mbengue, S.; Fusek, M.; Schwarz, J.; Vodička, P.; Šmejkalová, A.H.; Holoubek, I. Four Years of Highly Time Resolved Measurements of Elemental and Organic Carbon at a Rural Background Site in Central Europe. *Atmos. Environ.* **2018**, *182*, 335–346. [CrossRef]
69. Huang, Y.; Zhang, L.; Li, T.; Chen, Y.; Yang, F. Seasonal Variation of Carbonaceous Species of PM_{2.5} in a Small City in Sichuan Basin, China. *Atmosphere* **2020**, *11*, 1286. [CrossRef]
70. Ravindra, K.; Singh, T.; Mandal, T.K.; Sharma, S.K.; Mor, S. Seasonal Variations in Carbonaceous Species of PM_{2.5} Aerosols at an Urban Location Situated in Indo-Gangetic Plain and Its Relationship with Transport Pathways, Including the Potential Sources. *J. Environ. Manag.* **2022**, *303*, 114049. [CrossRef] [PubMed]
71. Sandrini, S.; Sandro, F.; Piazzalunga, A.; Prati, P.; Bonasoni, P.; Cavalli, F.; Bove, M.; Calvello, M.; Cappelletti, D.; Colombi, C.; et al. Spatial and Seasonal Variability of Carbonaceous Aerosol across Italy. *Atmos. Environ.* **2014**, *99*, 587–598. [CrossRef]
72. Bougiatioti, A.; Zampas, P.; Koulouri, E.; Antoniou, M.; Theodosi, C.; Kouvarakis, G.; Saarikoski, S.; Mäkelä, T.; Hillamo, R.; Mihalopoulos, N. Organic, Elemental and Water-Soluble Organic Carbon in Size Segregated Aerosols, in the Marine Boundary Layer of the Eastern Mediterranean. *Atmos. Environ.* **2013**, *64*, 251–262. [CrossRef]
73. Timonen, H.; Saarikoski, S.; Tolonen-Kivimäki, O.; Aurela, M.; Saarnio, K.; Petäjä, T.; Aalto, P.P.; Kulmala, M.; Pakkanen, T.; Hillamo, R. Size Distributions, Sources and Source Areas of Water-Soluble Organic Carbon in Urban Background Air. *Atmos. Chem. Phys.* **2008**, *8*, 5635–5647. [CrossRef]
74. Viana, M.; Maenhaut, W.; Chi, X.; Querol, X.; Alastuey, A. Comparative Chemical Mass Closure of Fine and Coarse Aerosols at Two Sites in South and West Europe: Implications for EU Air Pollution Policies. *Atmos. Environ.* **2007**, *41*, 315–326. [CrossRef]
75. Salma, I.; Mészáros, T.; Maenhaut, W. Mass Size Distribution of Carbon in Atmospheric Humic-like Substances and Water Soluble Organic Carbon for an Urban Environment. *J. Aerosol Sci.* **2013**, *56*, 53–60. [CrossRef]
76. Lee, H.-M.; Lee, S.P.; Li, Y.; Yu, J.Z.; Kim, J.Y.; Kim, Y.P.; Lee, J.Y. Characterization of Seasonal Difference of HULIS-C Sources from Water Soluble PM_{2.5} in Seoul, Korea: Probing Secondary Processes. *Aerosol Air Qual. Res.* **2021**, *21*, 200233. [CrossRef]
77. Qiao, T.; Zhao, M.; Xiu, G.; Yu, J. Seasonal Variations of Water Soluble Composition (WSOC, HULIS and WSIs) in PM₁ and Its Implications on Haze Pollution in Urban Shanghai, China. *Atmos. Environ.* **2015**, *123*, 306–314. [CrossRef]
78. Arruti, A.; Fernández-Olmo, I.; Irabien, A. Regional Evaluation of Particulate Matter Composition in an Atlantic Coastal Area (Cantabria Region, Northern Spain): Spatial Variations in Different Urban and Rural Environments. *Atmos. Res.* **2011**, *101*, 280–293. [CrossRef]
79. Ledoux, F.; Roche, C.; Delmaire, G.; Roussel, G.; Favez, O.; Fadel, M.; Courcot, D. Measurement Report: A 1-Year Study to Estimate Maritime Contributions to PM₁₀ in a Coastal Area in Northern France. *Atmos. Chem. Phys.* **2023**, *23*, 8607–8622. [CrossRef]

80. Chesselet, R.; Morelli, J.; Buat-Menard, P.; Orelli, J. Variations in Ionic Ratios between Reference Sea Water and Marine Aerosols. *J. Geophys. Res.* **1972**, *77*, 5116–5131. [[CrossRef](#)]
81. Su, B.; Wang, T.; Zhang, G.; Liang, Y.; Lv, C.; Hu, Y.; Li, L.; Zhou, Z.; Wang, X.; Bi, X. A Review of Atmospheric Aging of Sea Spray Aerosols: Potential Factors Affecting Chloride Depletion. *Atmos. Environ.* **2022**, *290*, 119365. [[CrossRef](#)]
82. Crawford, J.; Cohen, D.D.; Chambers, S.D.; Williams, A.G.; Atanacio, A. Impact of Aerosols of Sea Salt Origin in a Coastal Basin: Sydney, Australia. *Atmos. Environ.* **2019**, *207*, 52–62. [[CrossRef](#)]
83. Luo, L.; Zhang, Y.-Y.; Xiao, H.-Y.; Xiao, H.-W.; Zheng, N.-J.; Zhang, Z.-Y.; Xie, Y.-J.; Liu, C. Spatial Distributions and Sources of Inorganic Chlorine in PM_{2.5} across China in Winter. *Atmosphere* **2019**, *10*, 505. [[CrossRef](#)]
84. Hleis, D.; Fernández-Olmo, I.; Ledoux, F.; Kfoury, A.; Courcot, L.; Desmots, T.; Courcot, D. Chemical Profile Identification of Fugitive and Confined Particle Emissions from an Integrated Iron and Steelmaking Plant. *J. Hazard. Mater.* **2013**, *250–251*, 246–255. [[CrossRef](#)]
85. Cheng, B.; Ma, Y.; Li, H.; Feng, F.; Zhang, Y.; Qin, P. Water-Soluble Ions and Source Apportionment of PM_{2.5} Depending on Synoptic Weather Patterns in an Urban Environment in Spring Dust Season. *Sci. Rep.* **2022**, *12*, 21953. [[CrossRef](#)]
86. Ledoux, F.; Kfoury, A.; Delmaire, G.; Roussel, G.; El Zein, A.; Courcot, D. Contributions of Local and Regional Anthropogenic Sources of Metals in PM_{2.5} at an Urban Site in Northern France. *Chemosphere* **2017**, *181*, 713–724. [[CrossRef](#)]
87. Poulakis, E.; Theodosi, C.; Bressi, M.; Sciare, J.; Gherzi, V.; Mihalopoulos, N. Airborne Mineral Components and Trace Metals in Paris Region: Spatial and Temporal Variability. *Environ. Sci. Pollut. Res.* **2015**, *22*, 14663–14672. [[CrossRef](#)]
88. Fadel, M.; Courcot, D.; Seigneur, M.; Kfoury, A.; Oikonomou, K.; Sciare, J.; Ledoux, F.; Afif, C. Identification and Apportionment of Local and Long-Range Sources of PM_{2.5} in Two East-Mediterranean Sites. *Atmos. Poll. Res.* **2023**, *14*, 101622. [[CrossRef](#)]
89. Sillanpää, M.; Hillamo, R.; Saarikoski, S.; Frey, A.; Pennanen, A.; Makkonen, U.; Spolnik, Z.; Van Grieken, R.; Braniš, M.; Brunekreef, B.; et al. Chemical Composition and Mass Closure of Particulate Matter at Six Urban Sites in Europe. *Atmos. Environ.* **2006**, *40*, 212–223. [[CrossRef](#)]
90. Petit, J.-E.; Pallarès, C.; Favez, O.; Alleman, L.Y.; Bonnaire, N.; Rivière, E. Sources and Geographical Origins of PM₁₀ in Metz (France) Using Oxalate as a Marker of Secondary Organic Aerosols by Positive Matrix Factorization Analysis. *Atmosphere* **2019**, *10*, 370. [[CrossRef](#)]
91. Sterk, G.; Goossens, D. Emissions of Soil Dust and Related Problems in Europe: An Overview. In Proceedings of the Dustconf International Conference, Maastricht, The Netherlands, 23–24 April 2007.
92. Ni, T.; Li, P.; Han, B.; Bai, Z.; Ding, X.; Wang, Q.; Huo, J.; Lu, B. Spatial and Temporal Variation of Chemical Composition and Mass Closure of Ambient PM₁₀ in Tianjin, China. *Aerosol Air Qual. Res.* **2013**, *13*, 1832–1846. [[CrossRef](#)]
93. Rogula-Kozłowska, W.; Klejnowski, K.; Rogula-Kopiec, P.; Ośródk, L.; Krajny, E.; Błaszczak, B.; Mathews, B. Spatial and Seasonal Variability of the Mass Concentration and Chemical Composition of PM_{2.5} in Poland. *Air Qual. Atmos. Health* **2014**, *7*, 41–58. [[CrossRef](#)]
94. Wang, P.; Cao, J.; Shen, Z.; Han, Y.; Lee, S.; Huang, Y.; Zhu, C.; Wang, Q.; Xu, H.; Huang, R. Spatial and Seasonal Variations of PM_{2.5} Mass and Species during 2010 in Xi'an, China. *Sci. Total Environ.* **2015**, *508*, 477–487. [[CrossRef](#)]
95. Zhao, M.; Zhang, Y.; Ma, W.; Fu, Q.; Yang, X.; Li, C.; Zhou, B.; Yu, Q.; Chen, L. Characteristics and Ship Traffic Source Identification of Air Pollutants in China's Largest Port. *Atmos. Environ.* **2013**, *64*, 277–286. [[CrossRef](#)]
96. Viana, M.; Hammingh, P.; Colette, A.; Querol, X.; Degraeuwe, B.; de Vlieger, I.; van Aardenne, J. Impact of Maritime Transport Emissions on Coastal Air Quality in Europe. *Atmos. Environ.* **2014**, *90*, 96–105. [[CrossRef](#)]
97. Nigam, A.; Welch, W.; Miller, J.; Cocher, D.R., III. Effect of Fuel Sulphur Content and Control Technology on PM Emission from Ship's Auxiliary Engine. In Proceedings of the International Aerosol Conference, St. Paul, MN, USA, 10–15 September 2006; pp. 1531–1532.
98. Alves, C.; Evtugina, M.; Vicente, E.; Vicente, A.; Rienda, I.C.; de la Campa, A.S.; Tomé, M.; Duarte, I. PM_{2.5} Chemical Composition and Health Risks by Inhalation near a Chemical Complex. *J. Environ. Sci.* **2023**, *124*, 860–874. [[CrossRef](#)]
99. Penkała, M.; Ogrodnik, P.; Rogula-Kozłowska, W. Particulate Matter from the Road Surface Abrasion as a Problem of Non-Exhaust Emission Control. *Environments* **2018**, *5*, 9. [[CrossRef](#)]
100. Piscitello, A.; Bianco, C.; Casasso, A.; Sethi, R. Non-Exhaust Traffic Emissions: Sources, Characterization, and Mitigation Measures. *Sci. Total Environ.* **2021**, *766*, 144440. [[CrossRef](#)]
101. Ferrari, C.P.; Hong, S.; Van de Velde, K.; Boutron, C.F.; Rudniew, S.N.; Bolshov, M.; Chisholm, W.; Rosman, K.J.R. Natural and Anthropogenic Bismuth in Central Greenland. *Atmos. Environ.* **2000**, *34*, 941–948. [[CrossRef](#)]
102. Lam, K.S.; Cheng, Z.L.; Kot, S.C.; Tsang, C.W. Chemical Characteristics of Aerosols at Coastal Station in Hong Kong. II. Environmental Behavior of Trace Elements during the April 1995 to April 1996. *J. Environ. Sci. China* **2004**, *16*, 212–221. [[PubMed](#)]
103. Valotto, G.; Rampazzo, G.; Visin, F.; Gonella, F.; Cattaruzza, E.; Glisenti, A.; Formenton, G.; Tieppo, P. Environmental and Traffic-Related Parameters Affecting Road Dust Composition: A Multi-Technique Approach Applied to Venice Area (Italy). *Atmos. Environ.* **2015**, *122*, 596–608. [[CrossRef](#)]
104. von Uexull, O.; Skerfving, S.; Doyle, R.; Braungart, M. Antimony in Brake Pads—A Carcinogenic Component? *J. Clean. Prod.* **2005**, *13*, 19–31. [[CrossRef](#)]
105. Lin, Y.-C.; Tsai, C.-J.; Wu, Y.-C.; Zhang, R.; Chi, K.-H.; Huang, Y.-T.; Lin, S.-H.; Hsu, S.-C. Characteristics of Trace Metals in Traffic-Derived Particles in Hsuehshan Tunnel, Taiwan: Size Distribution, Potential Source, and Fingerprinting Metal Ratio. *SALAMEH* **2015**, *15*, 4117–4130. [[CrossRef](#)]

106. Mancilla, Y.; Mendoza, A. A Tunnel Study to Characterize PM_{2.5} Emissions from Gasoline-Powered Vehicles in Monterrey, Mexico. *Atmos. Environ.* **2012**, *59*, 449–460. [[CrossRef](#)]
107. Pant, P.; Harrison, R.M. Estimation of the Contribution of Road Traffic Emissions to Particulate Matter Concentrations from Field Measurements: A Review. *Atmos. Environ.* **2013**, *77*, 78–97. [[CrossRef](#)]
108. He, L.-Y.; Hu, M.; Huang, X.-F.; Yu, B.-D.; Zhang, Y.-H.; Liu, D.-Q. Measurement of Emissions of Fine Particulate Organic Matter from Chinese Cooking. *Atmos. Environ.* **2004**, *38*, 6557–6564. [[CrossRef](#)]
109. Khan, J.Z.; Sun, L.; Tian, Y.; Shi, G.; Feng, Y. Chemical Characterization and Source Apportionment of PM₁ and PM_{2.5} in Tianjin, China: Impacts of Biomass Burning and Primary Biogenic Sources. *J. Environ. Sci.* **2021**, *99*, 196–209. [[CrossRef](#)]
110. Salameh, D.; Detournay, A.; Pey, J.; Pérez, N.; Liguori, F.; Saraga, D.; Bove, M.C.; Brotto, P.; Cassola, F.; Massabò, D.; et al. PM_{2.5} Chemical Composition in Five European Mediterranean Cities: A 1-Year Study. *Atmos. Res.* **2015**, *155*, 102–117. [[CrossRef](#)]
111. Andreae, M.O.; Merlet, P. Emission of Trace Gases and Aerosols from Biomass Burning. *Glob. Biogeochem. Cycles* **2001**, *15*, 955–966. [[CrossRef](#)]
112. Favez, O.; El Haddad, I.; Piot, C.; Boréave, A.; Abidi, E.; Marchand, N.; Jaffrezo, J.-L.; Besombes, J.-L.; Personnaz, M.-B.; Sciare, J.; et al. Inter-Comparison of Source Apportionment Models for the Estimation of Wood Burning Aerosols during Wintertime in an Alpine City (Grenoble, France). *Atmos. Chem. Phys.* **2010**, *10*, 5295–5314. [[CrossRef](#)]
113. Waked, A.; Favez, O.; Alleman, L.Y.; Piot, C.; Petit, J.-E.; Delaunay, T.; Verlinden, E.; Golly, B.; Besombes, J.-L.; Jaffrezo, J.-L.; et al. Source Apportionment of PM₁₀ in a North-Western Europe Regional Urban Background Site (Lens, France) Using Positive Matrix Factorization and Including Primary Biogenic Emissions. *Atmos. Chem. Phys.* **2014**, *14*, 3325–3346. [[CrossRef](#)]
114. Favez, O.; Cachier, H.; Sciare, J.; Sarda-Estève, R.; Martinon, L. Evidence for a Significant Contribution of Wood Burning Aerosols to PM_{2.5} during the Winter Season in Paris, France. *Atmos. Environ.* **2009**, *43*, 3640–3644. [[CrossRef](#)]
115. Bruce, D.; Karl, M.; Herdis, L.; Christer, J.; Aarnio, M.; Karppinen, A.; Kukkonen, J.; Ketznel, M.; Peter, W. Estimating Domestic Wood Burning Emissions of Particulate Matter in Two Nordic Cities by Combining Ambient Air Observations with Receptor and Dispersion Models. *Chem. Ind. Chem. Eng. Q.* **2010**, *16*, 237–241. [[CrossRef](#)]
116. Reche, C.; Viana, M.; Amato, F.; Alastuey, A.; Moreno, T.; Hillamo, R.; Teinilä, K.; Saarnio, K.; Seco, R.; Peñuelas, J.; et al. Biomass Burning Contributions to Urban Aerosols in a Coastal Mediterranean City. *Sci. Total Environ.* **2012**, *427–428*, 175–190. [[CrossRef](#)]
117. Kauhaniemi, M.; Karppinen, A.; Härkönen, J.; Kousa, A.; Alaviippola, B.; Koskentalo, T.; Aarnio, P.; Elolähde, T.; Kukkonen, J. Evaluation of a Modelling System for Predicting the Concentrations of PM_{2.5} in an Urban Area. *Atmos. Environ.* **2008**, *42*, 4517–4529. [[CrossRef](#)]
118. Choochuay, C.; Pongpiachan, S.; Tipmanee, D.; Deelman, W.; Suttinun, O.; Wang, Q.; Xing, L.; Li, G.; Han, Y.; Palakun, J.; et al. Long-Range Transboundary Atmospheric Transport of Polycyclic Aromatic Hydrocarbons, Carbonaceous Compositions, and Water-Soluble Ionic Species in Southern Thailand. *Aerosol Air Qual. Res.* **2020**, *20*, 1591–1606. [[CrossRef](#)]
119. Sciare, J.; Oikonomou, K.; Favez, O.; Liakakou, E.; Markaki, Z.; Cachier, H.; Mihalopoulos, N. Long-Term Measurements of Carbonaceous Aerosols in the Eastern Mediterranean: Evidence of Long-Range Transport of Biomass Burning. *Atmos. Chem. Phys.* **2008**, *8*, 5551–5563. [[CrossRef](#)]
120. Zhang, X.; Liu, Z.; Hecobian, A.; Zheng, M.; Frank, N.H.; Edgerton, E.S.; Weber, R.J. Spatial and Seasonal Variations of Fine Particle Water-Soluble Organic Carbon (WSOC) over the Southeastern United States: Implications for Secondary Organic Aerosol Formation. *Atmos. Chem. Phys.* **2012**, *12*, 6593–6607. [[CrossRef](#)]
121. Suto, N.; Kawashima, H. Measurement Report: Source Characteristics of Water-Soluble Organic Carbon in PM_{2.5} at Two Sites in Japan, as Assessed by Long-Term Observation and Stable Carbon Isotope Ratio. *Atmos. Chem. Phys.* **2021**, *21*, 11815–11828. [[CrossRef](#)]
122. Rastogi, N.; Patel, A.; Singh, A.; Singh, D. Diurnal Variability in Secondary Organic Aerosol Formation over the Indo-Gangetic Plain during Winter Using Online Measurement of Water-Soluble Organic Carbon. *Aerosol Air Qual. Res.* **2015**, *15*, 2225–2231. [[CrossRef](#)]
123. Win, M.S.; Tian, Z.; Zhao, H.; Xiao, K.; Peng, J.; Shang, Y.; Wu, M.; Xiu, G.; Lu, S.; Yonemochi, S.; et al. Atmospheric HULIS and Its Ability to Mediate the Reactive Oxygen Species (ROS): A Review. *J. Environ. Sci.* **2018**, *71*, 13–31. [[CrossRef](#)] [[PubMed](#)]
124. Lin, P.; Engling, G.; Yu, J.Z. Humic-like Substances in Fresh Emissions of Rice Straw Burning and in Ambient Aerosols in the Pearl River Delta Region, China. *Atmos. Chem. Phys.* **2010**, *10*, 6487–6500. [[CrossRef](#)]
125. Samara, C.; Voutsas, D.; Kouras, A.; Eleftheriadis, K.; Maggos, T.; Saraga, D.; Petrakakis, M. Organic and Elemental Carbon Associated to PM₁₀ and PM_{2.5} at Urban Sites of Northern Greece. *Environ. Sci. Pollut. Res. Int.* **2014**, *21*, 1769–1785. [[CrossRef](#)] [[PubMed](#)]
126. Kim, W.; Lee, H.; Kim, J.; Jeong, U.; Kweon, J. Estimation of Seasonal Diurnal Variations in Primary and Secondary Organic Carbon Concentrations in the Urban Atmosphere: EC Tracer and Multiple Regression Approaches. *Atmos. Environ.* **2012**, *56*, 101–108. [[CrossRef](#)]
127. Yoo, H.Y.; Kim, K.A.; Kim, Y.P.; Jung, C.H.; Shin, H.J.; Moon, K.J.; Park, S.M.; Lee, J.Y. Validation of SOC Estimation Using OC and EC Concentration in PM_{2.5} Measured at Seoul. *Aerosol Air Qual. Res.* **2022**, *22*, 210388. [[CrossRef](#)]

128. Potier, E.; Waked, A.; Bourin, A.; Minvielle, F.; Péré, J.C.; Perdrix, E.; Michoud, V.; Riffault, V.; Alleman, L.Y.; Sauvage, S. Characterizing the Regional Contribution to PM₁₀ Pollution over Northern France Using Two Complementary Approaches: Chemistry Transport and Trajectory-Based Receptor Models. *Atmos. Res.* **2019**, *223*, 1–14. [[CrossRef](#)]
129. Viana, M.; Maenhaut, W.; ten Brink, H.M.; Chi, X.; Weijers, E.; Querol, X.; Alastuey, A.; Mikuška, P.; Večeřa, Z. Comparative Analysis of Organic and Elemental Carbon Concentrations in Carbonaceous Aerosols in Three European Cities. *Atmos. Environ.* **2007**, *41*, 5972–5983. [[CrossRef](#)]

Disclaimer/Publisher’s Note: The statements, opinions and data contained in all publications are solely those of the individual author(s) and contributor(s) and not of MDPI and/or the editor(s). MDPI and/or the editor(s) disclaim responsibility for any injury to people or property resulting from any ideas, methods, instructions or products referred to in the content.